"El saber de mis hijos hará mi grandeza"

UNIVERSIDAD DE SONORA

División de Ciencias Exactas y Naturales

Programa de Posgrado en Matemáticas

Approaches to the exploration of scenarios in infectious disease dynamics: Dengue and COVID-19

T E S I S

Que para obtener el grado académico de:

Doctor en Ciencias
(Matemáticas)

Presenta:

Mayra Rosalia Tocto Erazo

Directores de Tesis: Dr. Daniel Olmos Liceaga
Dr. José Arturo Montoya Laos

Hermosillo, Sonora, México, 24 de marzo de 2021

SINODALES

Dra. Gudelia Figueroa Preciado
Universidad de Sonora.

Dr. José del Carmen Jiménez Hernández
Universidad Tecnológica de la Mixteca.

Dr. José Arturo Montoya Laos
Universidad de Sonora.

Dr. Daniel Olmos Liceaga
Universidad de Sonora.

Dr. Roberto Alonso Sáenz Casas
Universidad de Colima

"El saber de mis hijos hará mi grandeza"

UNIVERSIDAD DE SONORA

ACTA DE EXAMEN DE GRADO

En la ciudad de Hermosillo, Sonora, siendo las 16:00 horas del día 24 de marzo de 2021, se reunieron en Plataforma Virtual de la Universidad de Sonora, los integrantes del jurado:

Dra. Gudelia Figueroa Preciado
Dr. Daniel Olmos Liceaga
Dr. José del Carmen Jiménez Hernández
Dr. Roberto Alonso Sáenz Casas
Dr. José Arturo Montoya Laos

bajo la presidencia del primero y fungiendo como secretario el último, para realizar el examen de grado del programa de Doctorado en Ciencias Matemáticas, a:

MAYRA ROSALIA TOCTO ERAZO

quien de acuerdo a la opción de examen de grado presentó una tesis individual titulada

Approaches to the exploration of scenarios in infectious disease dynamics: Dengue and COVID-19

El jurado, después de debatir entre sí reservada y libremente, emitió el siguiente dictamen:

APROBADO POR UNANIMIDAD

y para constancia se levantó la presente acta.

El saber de mis hijos hará mi grandeza

MAYRA ROSALIA TOCTO ERAZO
216230035

Acta: 24
Foja: 24
Libro: 1

Dra. Gudelia Figueroa Preciado
Presidente

Dr. José Arturo Montoya Laos
Secretario

Dr. Daniel Olmos Liceaga
Sinodal

Dr. José del Carmen Jiménez Hernández
Sinodal externo

Dr. Roberto Alonso Sáenz Casas
Sinodal externo

DR. JESÚS ADOLFO MINJÁREZ SOSA, Coordinador del Programa de Doctorado en Ciencias Matemáticas de la Universidad de Sonora, hace constar que las firmas que anteceden corresponden al jurado que intervino en el examen de grado.

Hermosillo, Sonora, a 24 de marzo de 2021

DR. JESÚS ADOLFO MINJÁREZ SOSA
Coordinador de programa

El saber de mis hijos hará mi grandeza
DIVISIÓN DE CIENCIAS EXACTAS Y NATURALES
Coordinación Posgrado en Matemáticas

Folio: 9853

Agradecimientos

A mis dos asesores de tesis, Dr. Daniel Olmos y Dr. José Montoya, por su gran apoyo, dedicación y paciencia.

Al Dr. Pablo Reyes del Colegio de Sonora por proveernos los datos georeferenciados que fueron una pieza fundamental en esta tesis. Además, un agradecimiento especial por sus valiosos comentarios sobre esta tesis.

A la Dra. Lucia Castro y al Dr. Saúl Díaz Infante por las diversas discusiones que fueron muy enriquecedoras.

A mi mamá que desde muy pequeña me apoyó en este largo camino hacia las matemáticas.

A mi papá que en esta última etapa ha sido un apoyo importante. Tu humildad es un gran ejemplo en mi vida.

A mis hermanos Diana, Maydi y Junior que han sido un gran ejemplo de lucha constante a pesar de las adversidades.

A mi esposo Adrian por su inmenso apoyo desde que decidí venir a estudiar a México.

A todos mis compañeros y amigos que conocí durante el posgrado y que me hicieron pasar momentos muy amenos.

Al Consejo Nacional de Ciencia y Tecnología (CONACYT) por la beca de manutención proporcionada.

A la Secretaria de Salud del Gobierno del Estado de Sonora por los datos proporcionados a través del proyecto DCEN-USO315002889 de la Universidad de Sonora.

A mi papito y mamita.

Contents

Preface

Infectious diseases are caused by organisms, such as bacteria, viruses, parasites, or fungi, and can be transmitted from one person to another or by vectors [1]. These diseases have caused epidemics and pandemics throughout history and in our own time. For example, the Spanish flu of 1918 is considered the worst pandemic that affected 500 million people, and it has been estimated between 17 and 50 million deaths worldwide [2]. Malaria is still an endemic disease in many African countries, but it has significantly decreased its mortality rate since 2000 [3]. Dengue is another endemic disease in more than 100 countries around the world, with the highest number of cases reported in 2019 [4]; particularly, more than 3.1 million dengue cases were reported in the Americas region during that year [5]. Currently, up to this document writing date, the COVID-19 pandemic has affected more than 100 million people worldwide and has caused the death of 2.2 million approximately [6].

These types of diseases do not only directly affect the health of individuals, but they also have an impact on the economy, resulting in significant losses [7]. For example, 170 million dollars approximately are spent by the Mexican government on dengue disease annually, without considering the long-term consequences of dengue, the impact on travel and tourism, among others [8]. Another example is COVID-19, which has caused serious damage to the world economy due to the strict measures implemented by governments to stop its spread [9]. Thus, these diseases are a serious public health problem, and their effects vary greatly by geographical area and populations, and low-income countries are the most affected [10].

Human mobility is a key factor in the study of infectious diseases. For example,

the air transport network has performed a critical role in the global spread of influenza and SARS [11]. The capacity for an infected human to rapidly travel between any two points on earth has contributed that infectious diseases can spread more effectively than at any other time in history [12]. At an urban scale, human mobility is often composed of commuting patterns between homes and places of employment, education, or commerce [13]. Thus, human mobility undeniably plays a crucial role in the temporal and spatial transmission dynamics of infectious diseases [14].

Due to the characteristics of infectious diseases spread, public health authorities are interested in understanding the demographic and environmental factors that help establish patterns of spread in space-time [15]. Geographic Information Systems (GIS) accomplish an important role in the study of infectious diseases. They allow the capture, manipulation, analysis, and visualization of demographic information on the population and the disease spread in space-time [15]. Thus, they can help to achieve a more comprehensive and real vision in public health. This type of tool allows us to have an approach to the spatio-temporal dynamics of infectious diseases; therefore, it is key to formulate hypotheses of mathematical models for disease transmission dynamics.

In mathematics, different tools have been used to attend the problem of infectious diseases. The mathematical models provide a better understanding of disease dynamics and can contribute to decision-making regarding the control measures [16]. In particular, mathematical models based on ordinary differential equations have been widely used to study different infectious diseases, in which the SIR model has been the basis of this modeling approach [17–36]. Also, these models usually provide a threshold value known as the basic reproductive number (R_0) that indicates both the disease severity and the endemic state existence.

The mathematical models have parameters that control the characteristics of the disease dynamics, such as the size and amplitude of the outbreaks, the acme value,

the R_0, among others. Nowadays, many works estimate model parameters based on available data from epidemics to obtain some characteristics of the outbreak such as the R_0 or to assess the control measures applied. In this context, most parameters are usually estimated (sometimes the initial conditions too) using the least-squares method [18, 20], the maximum likelihood estimation [19], and Bayesian inference [21, 22]. However, the parameter identifiability problem arises when multiple sets of parameter values produce a very similar model fit to the data. It can be attributed to the model structure or the lack of information in a data set [37].

Here we provide frameworks that allow analyzing control and mobility scenarios for infectious disease dynamics. In all cases, we use mathematical models based on systems of ordinary differential equations to represent the disease dynamics. On the one hand, a completely theoretical-numerical study is carried out to analyze mobility scenarios through a little-explored modeling approach. On the other hand, statistical methods are used to delimit appropriate study areas based on socio-economic and socio-demographic information and to estimate reasonable values for the model parameters. The inclusion of socio-economic and socio-demographic information resulted from discussions with researchers in public health. Finally, due to the parameter identifiability problem, an approach based on the Monte Carlo method is proposed to provide baseline scenarios and assess the applied control measures. In the following lines, we show a summary of each chapter.

Chapter 1 provides a framework to explore the effect of control measures for a dengue outbreak in an area of the north side of Hermosillo. For this, we use the classic host-vector model with control to represent the measures applied during the 2010 dengue outbreak: awareness of the human population, elimination of potential larval breeding sites, and spraying of adult mosquitoes. We delimit a study area with approximately homogeneous characteristics based on hierarchical cluster analysis and Geographic Information Systems. The model parameters are estimated through a Bayesian approach to find appropriate values for the control parameters and, thus,

explore some hypothetical scenarios to the outbreak. Based on the scenarios obtained, we observe that even applying measures early, the accumulated total of cases could have increased if the measures were not applied with the intensity necessary to stop the outbreak. Similarly, measures applied later could have generated both a cumulative higher and lower than the estimated according to the intensity of control measures.

Chapter 2 introduces an important factor, such as the daily mobility of people to the host-vector model. Here, we use a little-explored modeling approach for dengue dynamics based on a system of ordinary differential equations to study the effect of human movement on characteristics of dengue dynamics such as the endemic equilibria existence and the start, duration, and amplitude of the outbreak. The model considers that every day is divided into two periods: high-activity and low-activity. Periodic human movement between patches occurs in discrete times. Based on numerical simulations, we show unexpected scenarios such as the disease extinction in regions where the local basic reproductive number is greater than 1. Similarly, we obtain scenarios where outbreaks appear even the local basic reproductive numbers in these regions are less than 1, and their size depends on the length of high-activity and low-activity periods.

Chapter 3 analyzes mobility scenarios to assess the effect of the daily local stay on the variations of some characteristics of dengue dynamics, such as the transmission rates and the local basic reproductive numbers for the 2010 dengue outbreak in Hermosillo. For this, we use the two-patch mathematical model proposed in Chapter 2. Based on preliminary cluster analysis, we divide the city into two regions, the south and north sides, which determine each patch of the model. In this case, we use information about the economically active population density to define the two regions. We use a Bayesian approach to estimate the transmission rates and local basic reproductive numbers of some urban mobility scenarios where residents of each patch spend daily 100% (no human movement between patches), 75%, and 50% of their

day at their residence place. We obtain that the estimated transmission rates of the north side do not vary, and it is more likely that the local basic reproductive number to be greater than one for all three different scenarios. On the contrary, transmission rates of the south side have more weight in lower values when considering the human movement between patches compared to the uncoupled case. Moreover, local basic reproductive numbers less than 1 are not negligible for the south side.

Chapter 4 proposes a novel approach to obtain baseline scenarios for COVID-19 dynamics, which allowed us to study some characteristics of the dynamics in Hermosillo and to assess the mandatory lockdown applied. Because of the parameter identifiability problem previously mentioned, our approach consists of proposing different sets of distributions for the model parameters by three researchers. We select the distributions and their supports based on the knowledge of the researchers, the versatility of certain distributions, or the literature on COVID-19. We use a mathematical model for COVID-19 formulated in [38, 39] and choose the best solutions of the model based on a threshold value defined as the 50th percentile of the sum of squared errors generated by comparing the daily data of new cases of infected, hospitalized, ambulatory, and deaths with its counterpart obtained by the mathematical model. Here we only present the results based on the set of distributions proposed by the author of this manuscript. We obtain that the date median of the occurring time of the acme is close to the acme occurring time in Hermosillo. The results indicate that delaying the confinement measures for one or two weeks would have significantly increased the prevalence of cases and deaths.

It is important to mention that the material presented in Chapters 2, 3, and 4 was published in *Mathematical Biosciences*, *Applied Mathematical Modelling*, and *PLoSONE* journals, respectively, which can be seen in [39–41].

Chapter 1

Exploring the effect of dengue control measures: the 2010 dengue outbreak in Hermosillo, Mexico

1.1 Introduction

Dengue is a viral disease that affects approximately 390 million people worldwide each year, occurring mainly throughout the tropics [42]. To attend this problem, multifaceted interventions are recommended rather than individual ones. Therefore, a combination of government commitment, authority involvement, and community mobilization is the best option to control the disease [43]. However, community participation is a key element because the failure of dengue control in some regions is attributed to a significant lack of inhabitants participation [44]. Also, assessing prevention and control strategies is very important since that allows us to identify successes and shortcomings that can help improve the response to future outbreaks [45]. Thus, it is important to assess the real impact of the response of both authorities and inhabitants to an outbreak, although this is complex to do.

Hermosillo, situated in northwest Mexico, is an arid city with high temperatures in summer, an average August temperature of 38.3°C, and low annual rainfall [46]. Despite its characteristics, it is an endemic area for dengue. In 2010,

Hermosillo recorded the highest number registered by the Health Ministry of Sonora State in last years. According to the guidelines for epidemiological surveillance, municipal government reports, and local media [47–53], control measures were taken in the 2010 dengue outbreak, such as educational campaigns, indoor and outdoor spraying of insecticides, application of larvicides, elimination of potential breeding larval sites, among others. It is important to mention that the intensity of the measures applied was stronger in neighborhoods with the highest number of dengue cases [48–53]. In particular, a short-term plan was initiated in the 39th epidemiological week in the northern neighborhoods of the city. As shown in [54], the varying socio-economic and socio-demographic conditions in the city limited a homogeneous spatial spread of dengue cases. Therefore, these heterogeneous factors throughout the city increase the complexity to assess the response to the 2010 dengue outbreak.

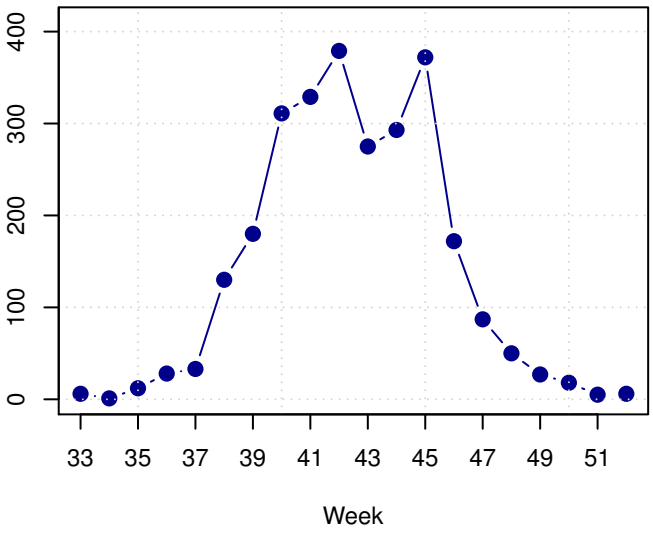

Figure 1.1: New confirmed cases of dengue per week in Hermosillo, 2010. Data from the Health Ministry of the State of Sonora.

In this chapter, we focus on exploring hypothetical scenarios for the application of dengue control measures in an area on the north side of Hermosillo. For this purpose, we use a basic mathematical model that considers three control measures: (i) awareness in the human population, (ii) elimination of potential larval breeding sites, and (iii) spraying of adult mosquitoes. We use real data to identify a study area with approximately homogeneous conditions by implementing hierarchical cluster analysis with socio-economic and socio-demographic data. We employ Bayesian inference to estimate model parameters. These estimated values are used to propose appropriate scenarios for the dengue outbreak under study.

1.2 Methods

1.2.1 Selection of the study area

According to data provided by the Health Ministry of the State of Sonora, Hermosillo recorded 2843 dengue-confirmed cases in 2010. In this study, we only consider the dengue cases with residence place, which represent 96% of cases (2729). Before the 33rd epidemiological week, there were only 15 confirmed cases. Figure 1.1 displays the temporal distribution of dengue cases from the 33rd to 52nd epidemiological week. We observe that there are two peaks of dengue cases in the 42nd and 45th week. This behavior may be related to heterogeneous characteristics through the city, such as socio-demographic and socio-economic features. Therefore, we select a study area with approximately homogeneous conditions to reduce the variability that the phenomenon exhibits.

To select an approximately homogeneous study area, we group AGEBs from Hermosillo with similar characteristics using hierarchical cluster analysis. In Mexico, an AGEB is a geographic area composed of a set of blocks and is the minimum census unit to obtain socio-demographic data. We select a set of socio-economic

and socio-demographic variables of the AGEBs according to the 2010 census data given by the National Institute of Statistics and Geography of Mexico (INEGI) and National Population Council (CONAPO) [55]. We only consider AGEBs whose selected variables for cluster analysis have complete information. These AGEBs contain 87.6% of the dengue cases. Figure 1.2 shows the grouping performed by the Ward method (Group 1 and Group 2). Figure 1.2 also contains AGEBs without complete information. AGEBs from Group 1 enclose 71.7% of the dengue cases, while Group 2, 15.9%. Table 1.2.1 displays some characteristics of groups according to used variables for cluster analysis. In general terms, the number of inhabitants per square kilometer of Group 1 is almost four times greater than Group 2. The percentage of the population with no health care of Group 1 is slightly higher than Group 2. The percentage of the population ≥ 25 years from Group 1 with at least 1 passing grade of higher education is approximately 11% smaller than Group 2. In addition, the percentage of households with internet in Group 1 is smaller than in Group 2. In Group 1, local health authorities reported 1958 confirmed dengue cases along 52 epidemiological weeks resulting in a rate of 44.1 cases/10 000 inhabitants, a very high rate compared to Group 2 (see Table 1). Therefore, the above characteristics suggest a special consideration of AGEBs from Group 1.

Based on the previous analysis, we establish the study area in the northeast side of Hermosillo, around the first case reported on week 33 from Group 1. Taking this case as a reference, we locate its AGEB and its nearby AGEBs that belong to the same group, see Figure 1.3(a). The selection of nearby AGEBs is based on the implementation of epidemiological fences when dengue cases are located in the community [47]. Thus, our study area is composed of 7 AGEBs and has a population of 31443 inhabitants. Figure 1.3(b) shows the temporal distribution of dengue cases from the selected area, where we can observe a peak of cases in the 40th week. There were 488 dengue cases along 20 epidemiological weeks, corresponding to a rate of 156.2 cases per 10,000 inhabitants in the study area. It is important to mention that

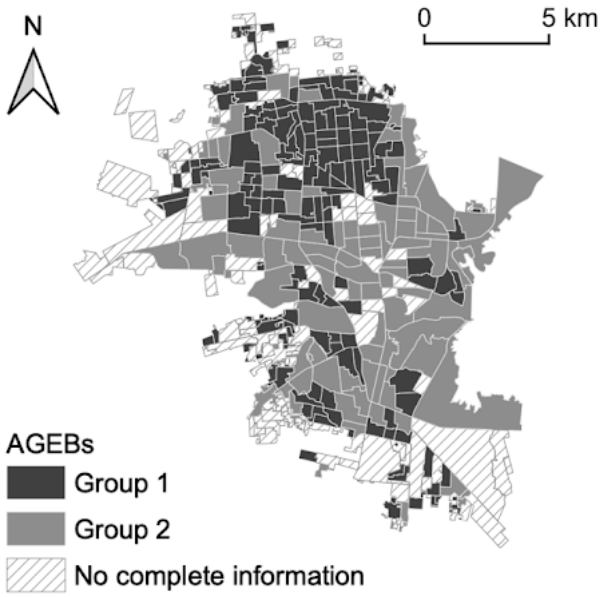

Figure 1.2: Grouping of AGEBs by cluster analysis.

the selected area contains the main focus of transmission of the outbreak [54].

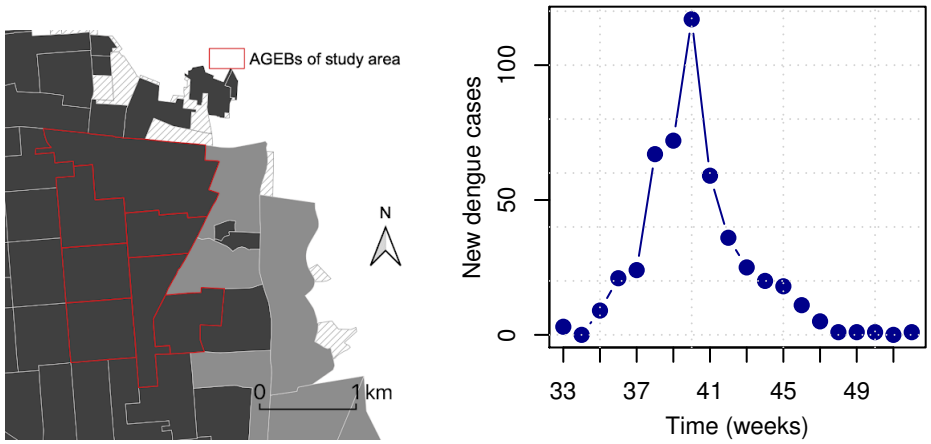

Figure 1.3: Study area. AGEBs of the study area marked by red lines (on the left side) and temporal distribution of the new confirmed cases of dengue per week marked by blue points (on the right side).

Characteristics	Group 1		Group 2	
	Total	%	Total	%
Demographic				
Total population	444 052	100.0	168 164	100.0
No health care	96 796	21.8	35 247	21.0
Population density (people per km^2)	8272.6	-	2254.2	-
Population $\geq$ 25 years	227 573	100.0	94 205	100.0
$\geq$ 1 passing grade of higher education	60 567	26.6	35 332	37.5
Households				
Occupied houses	119 531	100.0	46 377	100.0
With dirt floor	3669	3.1	1947	4.2
With piped water	116 501	97.5	44 954	96.9
With drainage	117 543	98.3	45 295	97.7
With car or truck	83 064	69.5	34 186	73.7
With internet	47 968	40.1	23 675	51.0
Index of marginalization	−0.764 (Low)		-0.762 (Low)	
Epidemiological data				
Dengue cases	1958	-	433	-
Rate per 10 000 inhabitants	44.1	-	25.7	-

Table 1.1: Characteristics of groups.

1.2.2 Mathematical model

We consider the classic vector-host model given in [56] as the basis of the mathematical model with a state-dependent control. We consider the following control measures (i) awareness of the human population, (ii) elimination of potential larval breeding sites, and (iii) spraying of insecticides. For this, we add class I_c, which represents the accumulated number of reported cases. The elimination of potential larval breeding sites is included by decreasing the recruitment rate of adult mosquitoes from Λ to $\kappa_0\Lambda$ after reaching a critical number of accumulated cases η. Similarly, spraying of insecticides included by increasing the mortality rate of adult mosquitoes from μ_v to $\omega_0\mu_v$ after reaching a critical number of reported accumulated cases η, that is, the average lifetime of mosquito decreases. On the other hand, awareness of the human

population is included by reducing the α_h and α_v transmission rates to $\beta\alpha_h$ and $\beta\alpha_v$, respectively, after reaching a critical number of reported accumulated cases η. Therefore, the vector-host model with a state-dependent control is given by:

$$\begin{aligned}
\dot{S}(t) &= -\frac{\beta\alpha_h S(t)V_i(t)}{N},\\
\dot{I}(t) &= \frac{\beta\alpha_h S(t)V_i(t)}{N} - \gamma I(t),\\
\dot{R}(t) &= \gamma I(t),\\
\dot{I}_c(t) &= \frac{\delta\beta\alpha_h S(t)V_i(t)}{N},\\
\dot{V}_s(t) &= \kappa\Lambda - \frac{\beta\alpha_v I(t)V_s(t)}{N} - \omega\mu_v V_s(t),\\
\dot{V}_i(t) &= \frac{\beta\alpha_v I(t)V_s(t)}{N} - \omega\mu_v V_i(t),
\end{aligned} \tag{1.1}$$

where $N = S + I + R$,

$$\beta = \begin{cases} 1, \text{ if } I_c(t) \leq \eta \\ \beta_0, \text{ if } I_c(t) > \eta \end{cases}, \kappa = \begin{cases} 1, \text{ if } I_c(t) \leq \eta \\ \kappa_0, \text{ if } I_c(t) > \eta \end{cases}, \omega = \begin{cases} 1, \text{ if } I_c(t) \leq \eta \\ \omega_0, \text{ if } I_c(t) > \eta \end{cases},$$

with $\beta_0 \in [0,1]$, $\kappa_0 \in [0,1]$, and $\omega_0 \geq 1$. Table 1.2 displays parameter definitions.

Parameter	**Definition**
N	Human population.
α_h	Transmission rate from mosquito to human.
α_v	Transmission rate from human to mosquito.
$1/\mu_v$	Average lifetime of mosquitoes.
$1/\gamma$	Average recovery time of humans.
Λ	Mosquito recruitment rate.
δ	Reporting rate.
β	Awareness rate.
η	Critical value of infected individuals.
κ	Elimination of breeding sites rate.
ω	Spraying of insecticides rate.

Table 1.2: Parameter definitions of model (1.1).

1.2.3 Parameter estimation

Let $V := V_s + V_i$ the total mosquito population, then

$$\lim_{t\to\infty} V(t) = \frac{\kappa\Lambda}{\omega\mu_v}.$$

We set initially that $V = \frac{\Lambda}{\mu_v}$ as the total mosquito population. Furthermore, if we assume that initially there are two mosquitoes per person, we have to $\Lambda = 2N\mu_v$. In addition, based on previous studies, we take that the average lifetime of a mosquito $(1/\mu_v)$ is 2 weeks, the reporting rate is 8% ($\delta = 0.08$) [57], and the average recovery time of humans $(1/\gamma)$ is 5 days [58]. Therefore, we use the data to estimate the remaining six parameters $(\alpha_h, \alpha_v, \beta, \eta, \kappa, \omega)$ by Bayesian inference approach.

Since the logarithmic transformations homogenize the variance and provide computational advantages to apply an MCMC method, we take logarithmic transformations as $\tilde{\alpha}_h = \log(\alpha_h)$ and $\tilde{\alpha}_v = \log(\alpha_v)$. Under this transformation we assume normality, which implies that the parameters follow a log-normal distribution. To establish the mean and standard deviation of the normal distributions for $\tilde{\alpha}_h$ and $\tilde{\alpha}_v$, we have taken values inside the reported range in [59]. Due to no information available for the control parameters, we establish the prior distributions given in Table 1.3. Then, the prior joint probability density function of $(\tilde{\alpha}_h, \tilde{\alpha}_v, \beta, \eta, \kappa, \omega)$ is given by

$$\pi(\tilde{\alpha}_h, \tilde{\alpha}_v, \beta, \eta, \kappa, \omega) = \pi(\tilde{\alpha}_h)\pi(\tilde{\alpha}_v)\pi(\beta)\pi(\eta)\pi(\kappa)\pi(\omega), \tag{1.2}$$

where $\pi(\bullet)$ is the probability density function of each parameter according to Table 1.3. Since model (1.1) is in a time-scale of days and starts at $t = 0$, we define D_i to represent the number of new infectious cases of dengue at ith week ($i = 33, ..., 52$), which is given by

$$D_{32+k} = \int_{7k-7}^{7k} \dot{I}_c(t)dt,$$

Parameter	Prior Distribution
$\tilde{\alpha}_h$	$\mathcal{N}(\log(0.3), 0.16)$
$\tilde{\alpha}_v$	$\mathcal{N}(\log(0.4), 0.09)$
β	$\mathcal{B}(24, 6)$
η	$\mathcal{U}(0, 250)$
κ	$\mathcal{B}(18, 27)$
ω	$\mathcal{U}(1, 5)$

Table 1.3: Prior Distribution for model parameters.

where $k = 1, 2, ..., 20$. Thus, we consider that the new weekly cases at week i follow a Poisson distribution with a mean $\lambda_i(\theta) = D_i$, where $\theta = (\tilde{\alpha}_h, \tilde{\alpha}_v, \beta, \eta, \kappa, \omega, \delta)$. Therefore, the sampling distribution is given by

$$\pi\left(\vec{x}|\theta\right) = \prod_{i=33}^{52} \frac{1}{x_i!} \left[\lambda_i\left(\theta\right)\right]^{x_i} \exp\left[-\lambda_i\left(\theta\right)\right], \tag{1.3}$$

where $\vec{x} = (x_{33}, x_{34}, ..., x_{52})$ are observed data. Therefore, the posterior distribution $\pi(\theta|\vec{x})$ is given by

$$\pi(\theta|\vec{x}) \propto \pi\left(\vec{x}|\theta\right) \pi(\theta),$$

where $\pi(\theta)$ and $\pi\left(\vec{x}|\theta\right)$ are given in (1.2) and (1.3), respectively.

We used an MCMC method based on the Metropolis-Hasting algorithm [60]. We run the algorithm for 200000 iterations, and use the last 50000 to generate samples of the model parameters. The initial conditions assumed are as follows: $S(0) = N_1 - 1$, $I(0) = 1$, $I_c(0) = 1$, $R(0) = 0$, $V_s(0) = \rho N$, $V_i(0) = 0$, where $N = 31443$.

1.3 Results

Figure 1.4 shows the scatter plot obtained by MCMC for control parameters (κ, ω, and β). In this figure, we can see the relationship between those parameters. For example, higher values of κ are related to higher values of ω as well as they are related

to higher values of β. That is to say, to observe the data under the model, a lower elimination of potential larval breeding sites is related to a higher mortality rate as well as it is related to lower awareness of the human population. Moreover, these values are related to a value of η (the blue to red color scale).

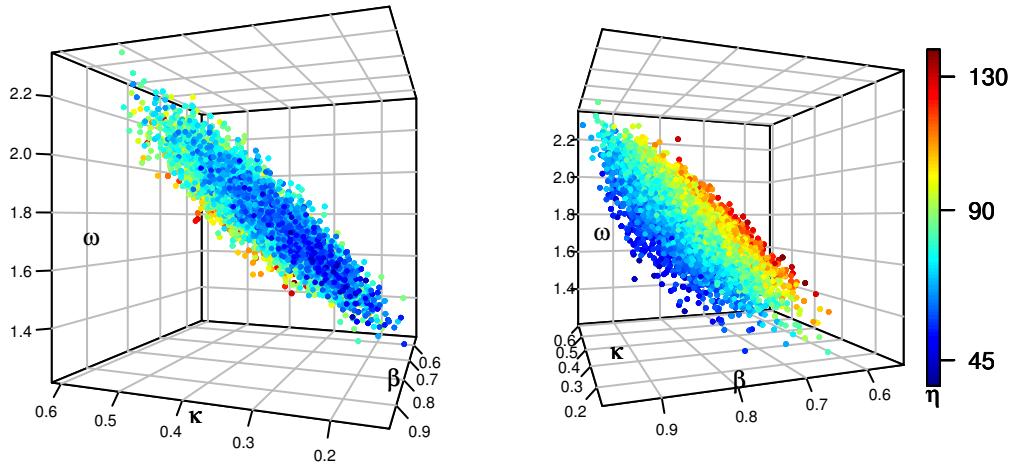

Figure 1.4: Scatter plot for control parameters κ, β, and ω seen from two different angles. The blue to red color scale indicates the corresponding value of η.

Parameter	**0.25 quantile** $(q_{0.25})$	**0.5 quantile** $(q_{0.5})$	**0.75 quantile** $(q_{0.75})$
α_h	0.15	0.17	0.20
α_v	0.24	0.29	0.34
β	0.77	0.81	0.85
η	71	80	89
κ	0.29	0.34	0.39
ω	1.67	1.77	1.86

Table 1.4: Quantile values of the posterior distributions for model parameters.

We use these obtained values as a framework for exploring hypothetical scenarios and comparing them with the estimated solution. For this, we use the 0.25, 0.5, and 0.75 quantiles of the posterior distributions obtained for model parameters shown in

Table 1.4. The 0.5 quantiles are used to define our estimated solution. Thus, we explore the dynamics of the cumulative number of cases according to the following scenarios:

Scenario 1. Control measures when it reaches a cumulative number of cases $\eta = 80$ (estimated value) with transmission rates reduced to 77% ($q_{0.25}$) and increased to 85% ($q_{0.75}$).

Scenario 2. Control measures when it reaches a cumulative number of cases $\eta = 71$ (value less than estimated) with transmission rates reduced to 77% ($q_{0.25}$) and increased to 85% ($q_{0.75}$).

Scenario 3. Control measures when it reaches a cumulative number of cases $\eta = 89$ (greater value than estimated) with transmission rates reduced to 77% ($q_{0.25}$) and increased to 85% ($q_{0.75}$).

In addition, we consider four intervention strategies given in Table 1.5 for each scenario.

Strategy	**Description**	κ	ω
I	Lower elimination of potential larval breeding sites combined with lower spraying of adult mosquitoes.	$q_{0.75}$	$q_{0.25}$
II	Higher elimination of potential larval breeding sites combined with lower spraying of adult mosquitoes.	$q_{0.25}$	$q_{0.25}$
III	Lower elimination of potential larval breeding sites combined with higher spraying of adult mosquitoes.	$q_{0.75}$	$q_{0.75}$
IV	Higher elimination of potential larval breeding sites combined with higher spraying of adult mosquitoes.	$q_{0.25}$	$q_{0.75}$

Table 1.5: Description of scenarios for control measures.

Figure 1.5 shows the accumulated number of cases according to Scenario 1 (A and B), Scenario 2 (C and D), and Scenario 3 (E and F). Also, in Figure 1.5-A, we can see the good fit of the model to the data (red line versus blue points). In general, we obtain better scenarios than the estimated solution (or similar) when both the

elimination of potential larval sites and the spraying of insecticides (Strategy IV) are intensified even applying the measures later. On the other hand, we have worse scenarios (or similar) than the estimated solution when the effectiveness of both strategies, the elimination of potential larval sites and the spraying of insecticides, decreases (Strategy I), even applying the measures early. Therefore, based on these proposed scenarios, applying measures early may not guarantee the reduction of cases unless certain control strategies are intensified.

According to the scenarios obtained, if the transmission rates had decreased by 85% combined with Strategies I or II, the total number of dengue cases would have increased. (see Figure 1.5-B). Furthermore, we would have observed more critical scenarios if the measures had been applied at the estimated value of η (equal to 80) or later ($\eta = 89$) combined with the transmission rates decrease to 85% and the application of Strategy I (see Figure 1.5-F). Thus, the delayed implementation of the control measures, combined with a reduction in their intensity, could have generated 50% more cases (blue solid line on Figure1.5-F). In addition, we observe scenarios with fewer accumulated cases if the measures had been applied earlier ($\eta = 71$) combined with a 77% reduction in transmission rates and Strategies III or IV, resulting in a decline of 33% of total cases (blue dotted line on Figure 1.5-C).

1.4 Conclussions and discussions

We have obtained hypothetical scenarios for a dengue outbreak that included the use of a mathematical model, a proceeding to delimit an appropriate study area, and statistical inference to estimate parameters. The purpose of using these tools together was to keep some aspects of the model close to a real context.

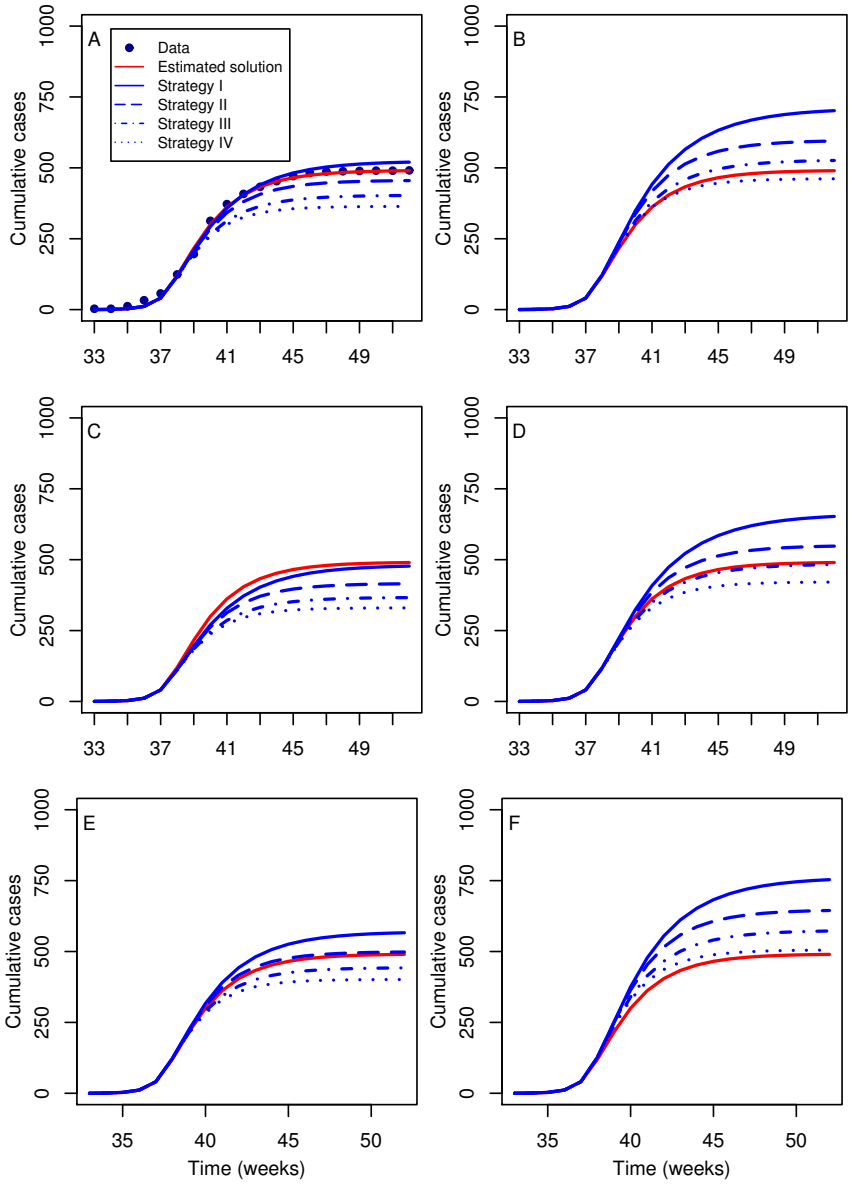

Figure 1.5: Hypothetical scenarios for control measure for $\eta = 80$ with transmission rates reduced to 77% (A) and increased to 85% (B), $\eta = 71$ with transmission rates reduced to 77% (C) and increased to 85% (D), and $\eta = 89$ with transmission rates reduced to 77% (E) and increased to 85% (F)

Based on the explored scenarios, decreasing the mortality rate of mosquitoes (Strategy III or IV) would have generated fewer cases in comparison to only increasing

the elimination of potential larval breeding sites, which coincides with [61]. In addition, the early application of a control measures mixing would have significantly decreased the total number of cases. However, in spite of applying control measures early, we would have obtained a higher number of cases compared to the estimated if control measures had not applied with the intensity necessary to stop the disease spread.

Previous works explore the impact of applying different control strategies for dengue [61–64], which are assessed separately or combined, and even some models consider seasonal factors. Here we use socio-economic and socio-demographic information to delimit an appropriate study area with similar conditions. This provided elements to estimate parameters and establish control scenarios over a region with approximately homogeneous characteristics. Moreover, the non-complex model was validated by the data, capturing the full dynamics of the outbreak.

Due to no available data on the mosquito population, some assumptions based on literature were made for the vector parameters. We also assumed that the control strategies for dengue were applied continuously. More detailed information on when and how the strategies were implemented could be useful to quantify the control measures. Thus, we could get a better approximation of the real impact of control strategies. In addition, it is important to mention that the η parameter is related to the time that the cumulative number of infected reaches a critical value. Therefore, it may be more relevant to describe this parameter in terms of time for decision-making in public health.

Here we have only explored some hypothetical scenarios in a delimited area of the city without considering the disease spread to contiguous neighborhoods. To analyze how it spread throughout the city, we would have to include human mobility. Some works study human mobility between regions to examine the effect of the application of control strategies to highly endemic areas [65, 66]. In the following

chapter, we study the impact of daily human movement based on a little-explored modeling approach.

Chapter 2

Effect of daily human movement on some characteristics of dengue dynamics*

2.1 Introduction

Dengue is an endemic disease in many countries around the world, mainly throughout the tropics [4, 42]. It is estimated that there are a total of 3.97 billion people at risk of dengue transmission [67]. Risk levels depend strongly on rainfall, temperature, and the degree of urbanization [42]. Human movement is also a key component of the transmission dynamics of many vector-borne diseases [68, 69]. For example, dengue infections have been related to travel to endemic places such as the Caribbean, South America, South-Central Asia, and Southeast Asia [70].

In urban areas, human movement is frequent and extensive but often composed of commuting patterns between homes and places of employment, education, or commerce [13]. At this scale, commuting people occur day-to-day, dominated by daily activities. In a study conducted at two factories in Bandung [71], authors suggest that some people may have acquired the dengue virus at work and not at home. Therefore, local human movement plays an important role in the temporal and spatial spread of the dengue disease.

*This article was published in Mathematical Biosciences, Vol. 332, Mayra R. Tocto-Erazo, Daniel Olmos-Liceaga and José A. Montoya-Laos, Effect of daily human movement on some characteristics of dengue dynamics, 108531, Copyright Elsevier (2020).

From the mathematical point of view, the role of the human movement on vector-borne diseases from various perspectives has been studied. In particular, ordinary differential equations have been used to model human mobility between two or more locations [25]. One approach is the continuous moving of the human population between places [26–31]. Other proposal is the residence time, which represents the proportion of time that humans budget their residence across regions [32–35]. However, a different approach is to consider the daily movement of people on the dynamics explicitly. This approach has been studied in [36], where the authors formulate a star-network of connections between a central city and peripheral villages. Also, they suppose the commute population is the same every day and the movement period to the central city is half a day. However, despite there are studies about the human movement from different approaches, it has been poorly understood.

In this work, our objective is to study the effect of the daily periodic movement on some characteristics of dengue dynamics, such as the existence of endemic equilibria and outbreaks (the start, duration and, amplitude). We formulate a two-patch model based on a system of ordinary differential equations and incorporate human daily movement, where movement takes place at periodic discrete times every day as in [36]. Every day is divided into two periods: low-activity and high-activity, which could represent night and day, respectively. We consider that the low-activity period represents the time interval where humans stay at their residence patch. The movement occurs during the high-activity period in which people commute to school, work, or other daily activities; also, high-activity period can be related to extraordinary events where large numbers of humans interact. To study this model, we first analyze the patches separately without considering a piecewise definition in time. Then, based on numerical simulations, we study the complete model to observe some effects of the periodic human movement on the dynamics.

This work is divided into the following sections. First, the formulation of the model and the analysis of uncoupled patches are given in Section 2.2. Then, in Section

2.3, we study the effect of daily human movement on some characteristics of model dynamics based on numerical studies under some scenarios. Finally, conclusions and discussions about our results are presented in Section 2.4.

2.2 Formulation of model

The classic vector-host mathematical model is given by the following system

$$\begin{aligned}
\dot{S}(t) &= \mu_h N - \frac{\beta S(t) Q(t)}{N} - \mu_h S(t), \\
\dot{I}(t) &= \frac{\beta S(t) Q(t)}{N} - (\delta + \mu_h) I(t), \\
\dot{R}(t) &= \delta I(t) - \mu_h R, \\
\dot{P}(t) &= \Lambda_v - \frac{\beta_v P(t) I(t)}{N} - \mu_v P(t), \\
\dot{Q}(t) &= \frac{\beta_v P(t) I(t)}{N} - \mu_v Q(t),
\end{aligned} \tag{2.1}$$

where S, I and, R represent the susceptible, infected, and recovered population, respectively, and P and Q the susceptible and infected mosquito population, respectively.

We include the daily periodic movement between two patches in model (2.1) as follows. The interval $[t_k, t_{k+1})$ is the time period corresponding to the kth day and $T_l \in (0, 1)$ the fraction of the day of *low-activity* such that for the interval $[t_k, t_k + T_l)$ we have in each patch only resident population composed of N_i individuals ($i = 1, 2$). Thus, the time interval $[t_k, t_k + T_l)$ is named the *low-activity* period. For a fixed day k, α_i represents the proportion of the population from patch i that moves every day to another patch j at time $t_k + T_l$ and returns to patch i at time t_{k+1}. Thus, human movement takes place on the time interval $[t_k + T_l, t_{k+1})$, which is named the *high-activity* period.

For the low-activity period, the susceptible, infected, and recovered human population from patch i are represented by S_i^l, I_i^l, and R_i^l, respectively. The susceptible and infected vector population from patch i are represented by P_i and Q_i, respectively. On the other hand, for the high-activity period, the human population from patch i is divided into two subpopulations. The first subpopulation is composed of people from patch i who do not move to another patch, that is, $(1-\alpha_i)N_i$. This subpopulation is subdivided into susceptible (S_{ii}^h), infected (I_{ii}^h), and recovered (R_{ii}^h). The second subpopulation is composed of residents from patch j who move to patch i, $\alpha_j N_j$. This subpopulation is subdivided into susceptible (S_{ji}^h), infected (I_{ji}^h), and recovered (R_{ji}^h). Since we assume that the vector population does not move between patches, susceptible and infected vectors remain represented by P_i and Q_i, respectively. Thus, the following equations represent the dynamics of the populations for the low-activity period $[t_k, t_k + T_l)$:

$$\begin{aligned}
\dot{S}_i^l(t) &= \mu_h N_i^l - \frac{\beta_i S_i^l(t) Q_i(t)}{N_i^l} - \mu_h S_i^l(t), \\
\dot{I}_i^l(t) &= \frac{\beta_i S_i^l(t) Q_i(t)}{N_i^l} - (\delta_i + \mu_h) I_i^l(t), \\
\dot{R}_i^l(t) &= \delta_i I_i^l(t) - \mu_h R_i^l(t), \\
\dot{P}_i(t) &= \Lambda_{vi} - \frac{\beta_{vi} P_i(t) I_i^l(t)}{N_i^l} - \mu_{vi} P_i(t), \\
\dot{Q}_i(t) &= \frac{\beta_{vi} P_i(t) I_i^l(t)}{N_i^l} - \mu_{vi} Q_i(t),
\end{aligned} \tag{2.2}$$

where $N_i^l := N_i$ and $i = 1, 2$.

Parameter	Definition
α_i	Proportion of humans from patch i who move to patch j at time $t_k + T_{la}$.
N_i	Resident humans of patch i.
$1/\mu_h$	Average lifetime of humans.
$1/\mu_{vi}$	Average lifetime of mosquitoes in patch i.
β_i	Transmission rate from mosquito to human in patch i.
β_{vi}	Transmission rate from human to mosquito in patch i.
$1/\delta_i$	Average recovery time of humans in patch i.
Λ_{vi}	Mosquito recruitment rate in patch i.

Table 2.1: Parameter definition of model (2.2)-(2.3).

For the high-activity period $[t_k + T_l, t_{k+1})$, the set of equations become:

$$\begin{aligned}
\dot{S^h_{ii}}(t) &= (1-\alpha_i)\mu_h N^l_i - \frac{\beta_i S^h_{ii}(t) Q_i(t)}{N^h_i} - \mu_h S^h_{ii}(t),\\
\dot{I^h_{ii}}(t) &= \frac{\beta_i S^h_{ii}(t) Q_i(t)}{N^h_i} - (\delta_i + \mu_h) I^h_{ii}(t),\\
\dot{R^h_{ii}}(t) &= \delta_i I^h_{ii}(t) - \mu_h R^h_{ii}(t),\\
\dot{S^h_{ji}}(t) &= \alpha_j \mu_h N^l_j - \frac{\beta_i S^h_{ji}(t) Q_i(t)}{N^h_i} - \mu_h S^h_{ji}(t),\\
\dot{I^h_{ji}}(t) &= \frac{\beta_i S^h_{ji}(t) Q_i(t)}{N^h_i} - (\delta_i + \mu_h) I^h_{ji}(t),\\
\dot{R^h_{ji}}(t) &= \delta_i I^h_{ji}(t) - \mu_h R^h_{ji}(t),\\
\dot{P}_i(t) &= \Lambda_{vi} - \frac{\beta_{vi} P_i(t)(I^h_{ii}(t) + I^h_{ji}(t))}{N^h_i} - \mu_{vi} P_i(t),\\
\dot{Q}_i(t) &= \frac{\beta_{vi} P_i(t)(I^h_{ii}(t) + I^h_{ji}(t))}{N^h_i} - \mu_{vi} Q_i(t),
\end{aligned} \tag{2.3}$$

where $N^h_i := (1-\alpha_i)N_i + \alpha_j N_j$, and $i, j = 1, 2, i \neq j$. All model parameters are defined in Table 2.1.

We observe that model (2.2)-(2.3) can be reduced to uncoupled patches in the form of system (2.1). This is done by taking $T_l = 1$, that is, having only low-activity

periods.

In order to study our coupled model (2.2)-(2.3), we first analyze each system separately without considering a piecewise definition in time. Then, we focus on understanding the dynamics of the daily human movement.

2.2.1 Uncoupled case

System (2.2) is positively invariant in $\Omega_i = \{(S_i^l, I_i^l, R_i^l, P_i, Q_i) \in \mathbb{R}^5 : S_i^l \geq 0,\ I_i^l \geq 0,\ R_i^l \geq 0,\ S_i^l + I_i^l + R_i^l = N_i^l,\ P_i \geq 0,\ Q_i \geq 0,\ P_i + Q_i \leq \Lambda_{v_i}/\mu_{v_i}\}$ [56]. Then, the disease-free equilibrium of system (2.2) is given by $(\bar{S}_i, \bar{I}_i, \bar{R}_i, \bar{P}_i, \bar{Q}_i) = (N_i^l, 0, 0, \Lambda_{v_i}/\mu_{v_i}, 0)$ and, using the next generation matrix approach as in [72], the basic reproductive number (R_{il}) of the uncoupled system is given by

$$R_{il} := \frac{\beta_i \beta_{v_i} \Lambda_{v_i}}{\mu_{v_i}^2 (\delta_i + \mu_h) N_i^l}.$$

Previous work [56] has shown that if $R_{il} > 1$, then there exists an endemic equilibrium $(\tilde{S}_i, \tilde{I}_i, \tilde{R}_i, \tilde{P}_i, \tilde{Q}_i)$, where

$$\tilde{S}_i = \frac{\mu_h (N_i^l)^2}{\beta_i \tilde{Q}_i + \mu_h N_i^l}, \qquad \tilde{I}_i = \frac{\beta_i \mu_h N_i^l \tilde{Q}_i}{(\beta_i \tilde{Q}_i + \mu_h N_i^l)(\delta_i + \mu_h)},$$

$$\tilde{R}_i = N_i^l - \tilde{S}_i - \tilde{I}_i, \qquad \tilde{P}_i = \frac{\Lambda_{v_i}(\beta_i \tilde{Q}_i + \mu_h N_i^l)(\delta_i + \mu_h)}{\beta_{vi}\beta_i \mu_h \tilde{Q}_i + \mu_{v_i}(\beta_i \tilde{Q}_i + \mu_h N_i^l)(\delta_i + \mu_h)},$$

$$\tilde{Q}_i = \frac{\mu_h \mu_{v_i} N_i^l (\delta_i + \mu_h)[R_{il} - 1]}{\beta_i [\beta_{v_i} \mu_h + \mu_{v_i}(\delta_i + \mu_h)]}.$$

In addition, authors in [56, 73] also have shown that the disease-free equilibrium is globally asymptotically stable (GAS) when $R_{il} < 1$, and the endemic equilibrium is GAS when $R_{il} > 1$.

For the high-activity period (2.3), we define $S_{i*} := S_{ii}^h + S_{ji}^h$, $I_{i*} := I_{ii}^h + I_{ji}^h$, $R_{i*} := R_{ii}^h + R_{ji}^h$, $N_i^h := S_{i*} + I_{i*} + R_{i*} = (1 - \alpha_i)N_i^l + \alpha_j N_j^l$. Thus, the dynamics of uncoupled system (2.3) can be written as:

$$
\begin{aligned}
\dot{S}_{i*}(t) &= \mu_h N_i^h - \frac{\beta_i S_{i*}(t) Q_i(t)}{N_i^h} - \mu_h S_{i*}(t),\\
\dot{I}_{i*}(t) &= \frac{\beta_i S_{i*}(t) Q_i(t)}{N_i^h} - (\delta_i + \mu_h) I_{i*}(t),\\
\dot{I}_{i*}(t) &= \delta_i I_{i*}(t) - \mu_h R_{i*}(t),\\
\dot{P}_i(t) &= \Lambda_{v_i} - \frac{\beta_{v_i} P_i(t) I_{i*}(t)}{N_i^h} - \mu_{v_i} P_i(t),\\
\dot{Q}_i(t) &= \frac{\beta_{v_i} P_i(t) I_{i*}(t)}{N_i^h} - \mu_{v_i} Q_i(t),
\end{aligned}
\tag{2.4}
$$

for each $i = 1, 2$.

Since the structure of system (2.4) is the same as (2.2), results concerning the stability of the equilibrium points are analogous to system (2.2). In particular, the disease-free and endemic equilibrium points are given by $(N_i^l, 0, 0, \Lambda_{v_i}/\mu_{v_i}, 0)$ and $(\tilde{S}_{i*}, \tilde{I}_{i*}, \tilde{R}_{i*}, \tilde{P}_{i*}, \tilde{Q}_{i*})$, respectively, where

$$
\tilde{S}_{i*} = \frac{\mu_h (N_i^h)^2}{\beta_i \tilde{Q}_{i*} + \mu_h N_i^h}, \qquad \tilde{I}_{i*} = \frac{\beta_i \mu_h N_i^h \tilde{Q}_{i*}}{(\beta_i \bar{Q}_i + \mu_h N_i^h)(\delta_i + \mu_h)},
$$

$$
\tilde{R}_{i*} = N_i^h - \tilde{S}_{i*} - \tilde{I}_{i*} \qquad \tilde{P}_{i*} = \frac{\Lambda_{v_i}(\beta_i \tilde{Q}_{i*} + \mu_h N_i^h)(\delta_i + \mu_h)}{\beta_{vi}\beta_i \mu_h \tilde{Q}_{i*} + \mu_{v_i}(\beta_i \tilde{Q}_{i*} + \mu_h N_i^h)(\delta_i + \mu_h)},
$$

$$
\tilde{Q}_{i*} = \frac{\mu_h \mu_{v_i} N_i^h (\delta_i + \mu_h)[R_{ih} - 1]}{\beta_i[\beta_{v_i}\mu_h + \mu_{v_i}(\delta_i + \mu_h)]}.
$$

In addition, the basic reproductive number (R_{ih}) for uncoupled system (2.4) is given by

$$
R_{ih} = \frac{\beta_i \beta_{v_i} \Lambda_{v_i}}{\mu_{v_i}^2 (\delta_i + \mu_h) N_i^h}.
$$

We observe that each local basic reproductive number R_{il} and R_{ih} depend on the actual number of individuals in patch i. In this sense, the theoretical results on the existence and stability of the equilibrium points are given for the uncoupled subsystems. However, when the patches are coupled, these local basic reproductive numbers lose meaning to describe the global dynamics and only provide appropriate

information about stability and existence of equilibria when the patches are uncoupled. It is important to mention that the solutions for the coupled case are non-negative and bounded (see proof in Appendix 2.A). Moreover, the bounds for the solutions are given by N_i^l and N_i^h for low-activity and high-activity periods, respectively. In this case, a global R_0 is not well defined and, therefore, we cannot have a measure for the global and coupled case. Thus, in order to provide information about the behavior of the coupled system, we will focus our understanding based on the theoretical values of the basic reproductive numbers for the uncoupled case.

2.3 Effect of daily human movement on the endemic levels and the outbreaks

In this section, we focus on understanding some effects due to daily human movement on the existence of the endemic equilibrium points and the outbreaks for coupled model (2.2)-(2.3). For this, we proceed to study such effects in three stages. In the first stage, we characterize the local basic reproductive number and the endemic equilibrium values of each patch as a function of the total population size to see how changes in the population affect both, the R_0 and equilibrium point values. In the second stage, we show the changes that the local basic reproductive numbers in each patch may experiment after migration. Finally, in the last stage, based on numerical studies, we evidence the effects of daily human movement on some characteristics of the dynamics, such as the existence and disappearance of endemic equilibria, duration, size and peak of the outbreak.

2.3.1 Dependence on the basic reproductive number and the endemic equilibria as a function of population size

In general, the basic reproductive number (R_0) and the endemic equilibrium (I^*) of model (2.2)-(2.3) for a disconnected patch with human population N can be written as

$$R_0 = \frac{\beta\beta_v\Lambda_v}{\mu_v^2(\delta+\mu_h)N} \tag{2.5}$$

and

$$I^* = \frac{\beta\mu_h N Q^*}{(\beta Q^* + \mu_h N)(\delta+\mu_h)}, \text{ where } Q^* = \frac{\mu_h\mu_v N(\delta+\mu_h)[R_0-1]}{\beta[\beta_v\mu_h + \mu_v(\delta+\mu_h)]}. \tag{2.6}$$

From (2.5) and (2.6), we have that $R_0 = 1$ at a point $\overline{N} = \beta\beta_v\Lambda_v/[\mu_v^2(\delta+\mu_h)]$, and I^* reaches its maximum at point $\hat{N}$ is given by

$$\hat{N} = \frac{-2\mu_v^2\beta\Lambda_v a + 2\mu_v\beta\Lambda_v\sqrt{\mu_v^2a^2 + \mu_h\mu_v\beta_v a}}{2\mu_h\mu_v^3 a},$$

where $a = \delta + \mu_h$. From Figure 2.1, we observe that a patch with N smaller (larger) than $\overline{N}$ leads to have $R_0 > 1$ ($R_0 < 1$). The basic reproductive number is a measure that gives conditions for the existence of endemic equilibria and disease propagation in each patch separately. Thus, $R_0 < 1$ means that there is no favorable conditions for the disease spread, whereas $R_0 > 1$ implies that the conditions are favorable for an outbreak in each disconnected patch. In addition, while $N < \hat{N}$, the value of the endemic equilibrium I^* increases as N grows up and decreases when $N > \hat{N}$.

2.3.2 Changes in R_0 after one migration process

The findings in the previous subsection can be applied to see how the disease propagation conditions change in each patch when there is human migration between them. For this, we define A as the difference between the population that moves from patch 1 to patch 2 and the population that moves from patch 2 to patch 1, that

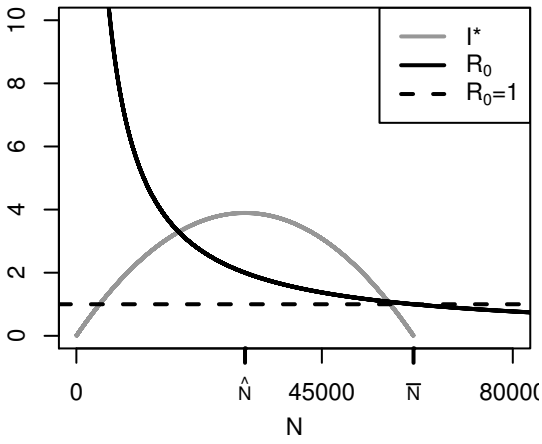

Figure 2.1: R_0 and I^* versus N. Parameter values: $\Lambda_v = 1200$, $\beta = 0.25$, $\beta_v = 0.15$, $\mu_h = 0.000036$, $\mu_v = 0.0714$, and $\delta = 0.1428$.

is, $A := \alpha_1 N_1^l - \alpha_2 N_2^l$. Table 2.2 shows a list of possible outcomes of the basic reproductive numbers after the interchange of populations from one patch to another. In general, the results of Table 2 are based on how many individuals we need to move from one patch to another (the value of A) in order to have our population N_i^h smaller or larger than the threshold value $\overline{N}$ given that N_i^l is smaller or larger than $\overline{N}$. The first column of the table shows the value of the basic reproductive number in each patch before migration is considered (R_{1l} and R_{2l}). The second column shows the possible outcomes after a proportion of humans from patch 1 moves to patch 2, and vice versa (R_{1h} and R_{2h}). The third column displays the conditions that the populations must satisfy in order for every scenario to occur. The scenarios are used to understand the daily human movement between patches. Some of the conditions given in Table 2.2 are explained in detail in Appendix 2.B. In order to show how the displacement of people from one patch to another may influence the disease propagation conditions, we examine the scenario $R_{1l} < 1$ and $R_{2l} > 1$, that is, during the low-activity period, in patch 1, the disease propagation conditions are not favorable, and in patch 2, the conditions are favorable. To this, we consider the following resident populations: $N_1^l = 90000$ and $N_2^l = 45000$ for patch 1 and 2,

Scenarios before migration	Scenarios after migration	Conditions
(1) $R_{1l} < 1$ and $R_{2l} > 1$	(a) $R_{1h} < 1$ and $R_{2h} < 1$	$\overline{N} - N_2^l < A < N_1^l - \overline{N}$
	(b) $R_{1h} < 1$ and $R_{2h} > 1$	$A < \min\left\{N_1^l - \overline{N}, \overline{N} - N_2^l\right\}$
	(c) $R_{1h} > 1$ and $R_{2h} < 1$	$A > \max\left\{N_1^l - \overline{N}, \overline{N} - N_2^l\right\}$
	(d) $R_{1h} > 1$ and $R_{2h} > 1$	$N_1^l - \overline{N} < A < \overline{N} - N_2^l$
(2) $R_{1l} < 1$ and $R_{2l} < 1$	(a) $R_{1h} < 1$ and $R_{2h} < 1$	$\overline{N} - N_2^l < A < N_1^l - \overline{N}$
	(b) $R_{1h} < 1$ and $R_{2h} > 1$	$A < \overline{N} - N_2^l$
	(c) $R_{1h} > 1$ and $R_{2h} < 1$	$A > N_1^l - \overline{N}$
	(d) $R_{1h} > 1$ and $R_{2h} > 1$	It is not possible
(3) $R_{1l} > 1$ and $R_{2l} > 1$	(a) $R_{1h} > 1$ and $R_{2h} > 1$	$N_1^l - \overline{N} < A < \overline{N} - N_2^l$
	(b) $R_{1h} > 1$ and $R_{2h} < 1$	$A > \overline{N} - N_2^l$
	(c) $R_{1h} < 1$ and $R_{2h} > 1$	$A < N_1^l - \overline{N}$
	(d) $R_{1h} > 1$ and $R_{2h} > 1$	It is not possible

Table 2.2: Possible scenarios for R_{1h} and R_{2h} after population exchange.

respectively, and parameter values given in Table 2.3. Based on the parameter values, we obtain that $R_{1l} = 0.68$ and $R_{2l} = 1.37$. Figure 2.2 shows under which conditions R_{1h} and R_{2h} are smaller or greater than 1, where the latter results in the existence of endemic equilibria according to α_1 and α_2 values. Note that Figure 2.2 shows only the first three outcomes for the case $R_{1l} < 1$ and $R_{2l} > 1$ given by Table 2.2. Observe that there are no values of α_1 and α_2 where both R_{1h} and R_{2h} are simultaneously greater than 1. From now on, to study the effect of daily periodic movement with complete model (2.2)-(2.3), we take variables I_1 and I_2 to represent infected residents from patches 1 and 2, respectively. That is,

$$I_i(t) = \begin{cases} I_i^l(t) & \text{if } t \in [t_k, t_k + T_l), \\ I_{ii}^h(t) + I_{ij}^h(t) & \text{if } t \in [t_k + T_l, t_{k+1}). \end{cases} \tag{2.7}$$

Parameter	Value
μ_h	0.000036
μ_{v1}, μ_{v2}	0.0714
β_1, β_2	0.25
β_{v1}, β_{v2}	0.15
δ_1, δ_2	0.1428
Λ_{v1}, Λ_{v2}	1200

Table 2.3: Parameter values for the different scenarios. All parameter values are taken from [59].

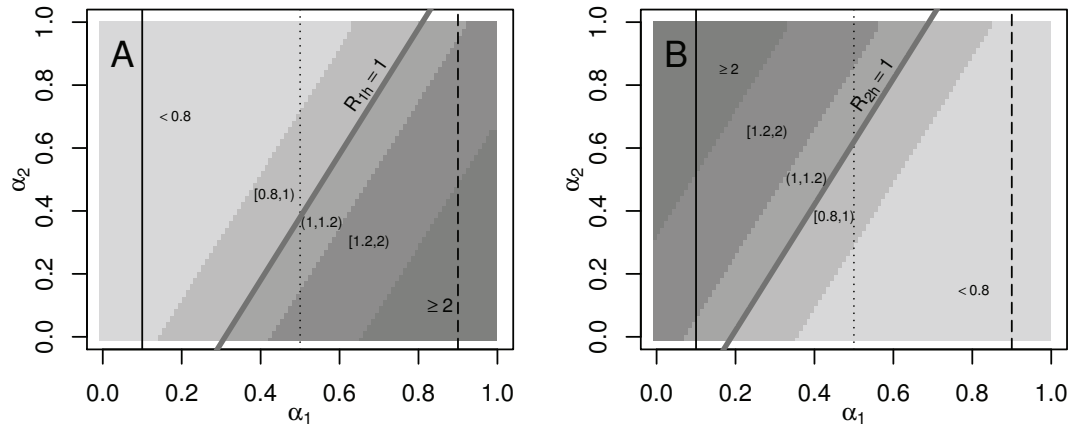

Figure 2.2: Value regions for R_{1h} and R_{2h} according to the α_1 and α_2 values for the scenario $R_{1l} < 1$ and $R_{2l} > 1$ in (**A**) patch 1 and (**B**) patch 2. The thick gray lines denote the region where $R_{1h} = 1$ (**A**) and $R_{2h} = 1$ (**B**). The vertical black lines represent the scenarios that will be studied in the next section.

for $i, j = 1, 2$, $i \neq j$. Observe that I_i counts the infected individuals from patch i, no matter where the disease was acquired, which is consistent with the information collected by the epidemiological surveillance systems.

2.3.3 Numerical studies

In this subsection, we study, by means of numerical simulations, some effects of daily human movement on characteristics of the coupled model solutions, such as the existence of endemic equilibria, and the start, duration, and amplitude of the outbreak.

2.3.3.1 Disappearance and appearance of endemic equilibria

Here we show the importance of T_l, α_1, and α_2 on the existence of endemic equilibria when $R_{1l} < 1$ and $R_{2l} > 1$. We present numerical simulations for different combinations of these parameters to observe whether or not the existence of endemic equilibria of the uncoupled patches is preserved. Here we study the following cases of the presented scenario in Figure 2.2: $\alpha_1 = 0.1$ (black solid line), $\alpha_1 = 0.5$ (black dotted line), and $\alpha_1 = 0.9$ (black dashed line), and for every case, we vary α_2 in $[0, 1]$ and T_l in $[0.1, 0.9]$. Figures 2.3 to 2.6 summarize the results of these experiments where we show the values of asymptotic solutions of I_1 and I_2 regarding α_2 and T_l. These values will give us an endemic state or a disease-free state.

- **Case** $\alpha_1 = 0.1$

  From Figure 2.2, theoretically $R_{1l} < 1$ and $R_{1h} < 1$, that is, there are no favorable conditions at any time during the day in patch 1 for an endemic equilibrium to exist. However, from Figure 2.3, there exists an endemic equilibrium of patch 1 for almost any combination of α_2 and T_l values. Taking $\alpha_1 = 0.1$, that is, 10% of individuals from patch 1 move to patch 2, generates endemic levels in patch 1. In general, while the resident people from patch 2 spend more time every day in their own patch, the dynamics are dominated by the theoretical values of R_{2l} and R_{2h}, which are greater than 1. From Figure 2.3, for values of α_2 close to 1 and T_l approximately 0.5, the opposite scenario

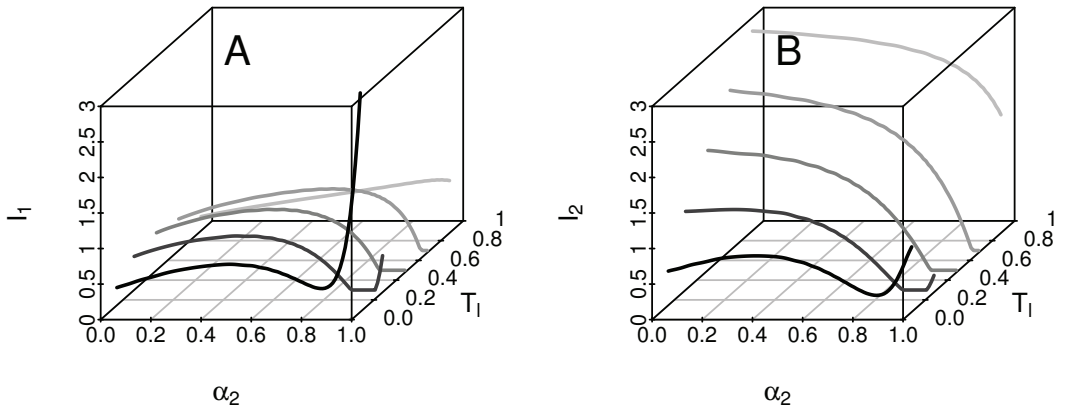

Figure 2.3: Existence of endemic equilibria for (**A**) I_1 and (**B**) I_2, against α_2 and T_l for case $\alpha_1 = 0.1$. Population sizes $N_1^l = 90000$ and $N_2^l = 45000$.

also occurs. If in a patch there are favorable conditions for the existence of endemic levels all the time ($R_{2l} > 1$ and $R_{2h} > 1$), we might get no endemic equilibrium in any patch. To get a better understanding of this phenomenon, we examine the behavior of the endemic equilibrium from patches when $\alpha_2 = 1.0$. Figure 2.4 shows the existence of endemic equilibria of I_1 and I_2 for $N_1^l = 90000$ with $N_2^l = 45000$ (black solid lines) and $N_2^l = 18000$ (black dashed lines) when $\alpha_1 = 0.1$ and $\alpha_2 = 1.0$. For $N_1^l = 90000$ and $N_2^l = 45000$, we have that $R_{1l} = 0.68$, $R_{2l} = 1.37$, $R_{1h} = 0.49$ and $R_{2h} = 6.86$. We observe a set of T_l values where the disease disappears in both patches when $N_2^l = 45000$. This phenomenon is explained as follows. Since $\alpha_1 = 0.1$ and $\alpha_2 = 1.0$, then, at the beginning of the high-activity period, 10% of the population from patch 1 moves to patch 2 and the whole population from patch 2 moves to patch 1. In the extreme case $T_l = 0.9$ (the low-activity period is very large), there is an endemic equilibrium in patch 2 due to the fact that almost all the time the population remains in their residence patch and the basic reproductive number (R_{2l}) is greater than 1. In this case, we could approximate the R_0 value of

patch 2 by the R_0 value of the disconnected patches. For individuals residing in patch 1, we observe that by taking 10% of individuals from patch 1 who move to patch 2, for a short time period, it is sufficient to generate endemic levels in patch 1 despite theoretically R_{1l} and R_{1h} are less than 1. Now, for the extreme case $T_l = 0.1$ (short low-activity period), the presence of an endemic level in patch 1 is due to the fact that most of the time the 10% of the population that belongs to patch 1, is in patch 2. This 10% carries the endemic levels acquired from patch 2 to patch 1. The endemic levels in patch 2 are due to the presence of endemic levels of mosquitoes that are present in the medium due to the 10% of individuals from patch 1. Finally, for intermediate values of T_l, the disease disappears in both patches. For this scenario, both the resident individuals from patch 2 and the visiting population from patch 1 spend almost the same time in each patch. As the basic reproductive numbers are smaller than 1 in patch 1 and larger than 1 in patch 2, we need to know why the disease cannot be sustained by patch 2. When populations are in patch 2, they do not stay long enough to increase the number of new infected individuals significantly. When individuals move to patch 1, the infective process is much less than in patch 2 (as $R_{1l} = 0.68 < 1$ and $R_{1h} = 0.49 < 1$) and new infections are imperceptible as the corresponding values of the basic reproductive numbers are very small and not close to 1. The overall effect leads to having a small enough infection rate compared to the disease recovery process and the disease disappears in both patches. However, from Figure 2.4, this region of disease extinction disappears when N_2^l decreases to 18000 (black dashed lines). In this case, we have that R_{1h} goes up from 0.49 to 0.62 and the region of disease extinction disappears.

- **Cases $\alpha_1 = 0.5$ and $\alpha_1 = 0.9$**

  Similar behavior of existence and non-existence of endemic equilibria arise for these values of α_1 and scenario $R_{1l} < 1$ and $R_{2l} > 1$.

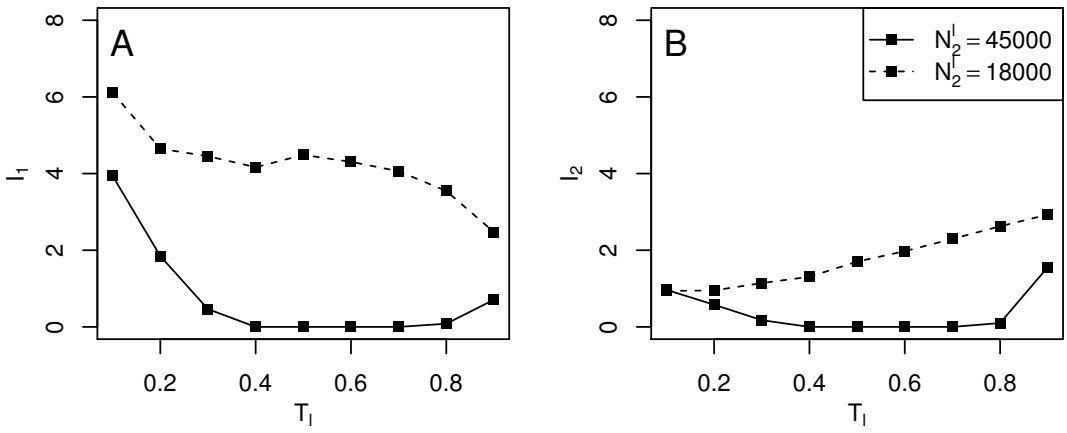

Figure 2.4: Existence of endemic equilibria for (**A**) I_1 and (**B**) I_2, for $\alpha_1 = 0.1$ and $\alpha_2 = 1.0$, and population sizes from patch 2 as $N_2^l = 45000$ (black solid line) and $N_2^l = 18000$ (black dashed line).

Figure 2.5 displays the existence of endemic equilibria of infected residents I_1 and I_2 for $\alpha_1 = 0.5$. There are endemic levels in both patches for long periods of low-activity ($T_l \geq 0.7$), except for some values of α_2 and T_l. In this case ($\alpha_1 = 0.5$), the region of disease extinction is larger than case $\alpha_1 = 0.1$. Here, the effect of human movement is more pronounced due to the fact that, for $\alpha_1 = 0.5$, the values of the basic reproductive numbers for the high-activity period in both patches are in the interval $[0.68, 1.37]$, whereas for $\alpha_1 = 0.1$, even though R_{1h} is smaller than 1 ($R_{1h} \in [0.49, 0.76]$), R_{2h} takes values in the interval $[1.14, 6.54]$ (see Figure 2.2).

Regions of disease extinction can be more complex as is observed in Figure 2.5, which shows the existence of endemic equilibria of I_1 and I_2 in case $\alpha_1 = 0.9$. As in the case $\alpha_1 = 0.1$ and $\alpha_1 = 0.5$, although there are favorable conditions for the existence of endemic equilibria in one of the patches during the low-activity period, the disease disappears for a set of values of α_2 and T_l. For this scenario, the values of R_{1h} and R_{2h} are opposite to R_{1l} and R_{2l}, that is, $R_{1h} > 1$ and

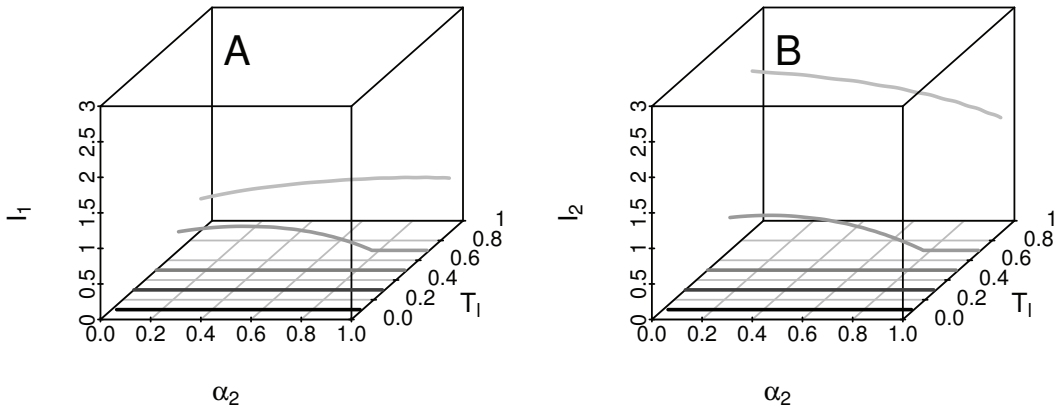

Figure 2.5: Existence of endemic equilibria for (**A**) I_1 and (**B**) I_2, against α_2 and T_l for case $\alpha_1 = 0.5$. Population sizes $N_1^l = 90000$ and $N_2^l = 45000$.

$R_{2h} < 1$. Clearly, depending on the settings of parameters α_1, α_2, T_l and the intensity of the basic reproductive numbers (values of R_{1l}, R_{2l}, R_{1h}, and R_{2h}), different regions of disease extinction can be obtained as observed in Figure 2.6.

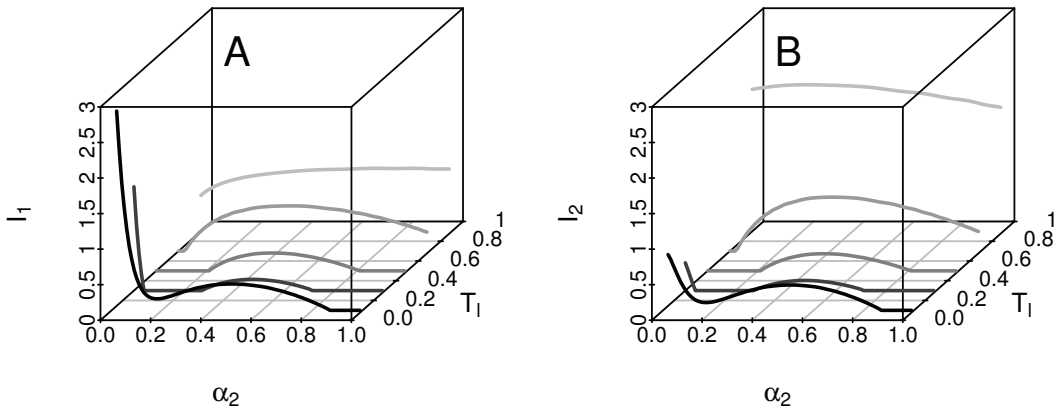

Figure 2.6: Existence of endemic equilibria for (**A**) I_1 and (**B**) I_2, against α_2 and T_l for case $\alpha_1 = 0.9$. Population sizes $N_1^l = 90000$ and $N_2^l = 45000$.

2.3.3.2 Effect on the outbreaks

In this subsection, we present scenarios to observe some effects of the periodic human movement on the outbreak dynamics. For this, we will use the variables I_1 and I_2 defined in equation (2.7), which represent the infected residents of patches 1 and 2, respectively, and the parameter values from Table 2.3 for the numerical simulations. Further, small population sizes for patches (N_1^l and N_2^l between 15000 and 90000 inhabitants for all simulations) are taken because we assumed the daily movement of people within a city, where the concept of patch can be seen as neighborhoods or city regions with similar demographic or socio-economic properties.

- **Disappearance of outbreaks**

  We first explore the scenario given in Subsection 2.3.3.1, where conditions for the emergence of an outbreak exist only in one of the patches. The purpose is to analyze the complete outbreak in a scenario where the disease disappears.

  As shown in Figure 2.3, there are no endemic equilibria in any patch for α_2 values close to 1 and T_l in $[0.4, 0.7]$. From Figure 2.7, we observe that there is an outbreak in patch 2 but not in patch 1 when the patches are uncoupled (see dashed lines), which coincides with the fact that $R_{1l} < 1$ and $R_{2l} > 1$ ($R_{1l} = 0.68$ and $R_{2l} = 1.37$). If we take $\alpha_1 = 0.1$ and $\alpha_2 = 1.0$, implies that $R_{1h} = 0.49$ and $R_{2h} = 6.86$. Under this scenario, from Figure 2.7, we notice there are outbreaks in both patches for very long periods of high-activity ($T_l = 0.1$) and very long periods of low-activity ($T_l = 0.9$). However, for T_l values in $[0.4, 0.7]$, outbreaks disappear in both patches. That means that this combination of parameters affects not only the existence of endemic equilibria but also the complete existence of the outbreak.

- **Emergence of outbreaks**

  Here we show the scenario where even though there are no conditions in any of

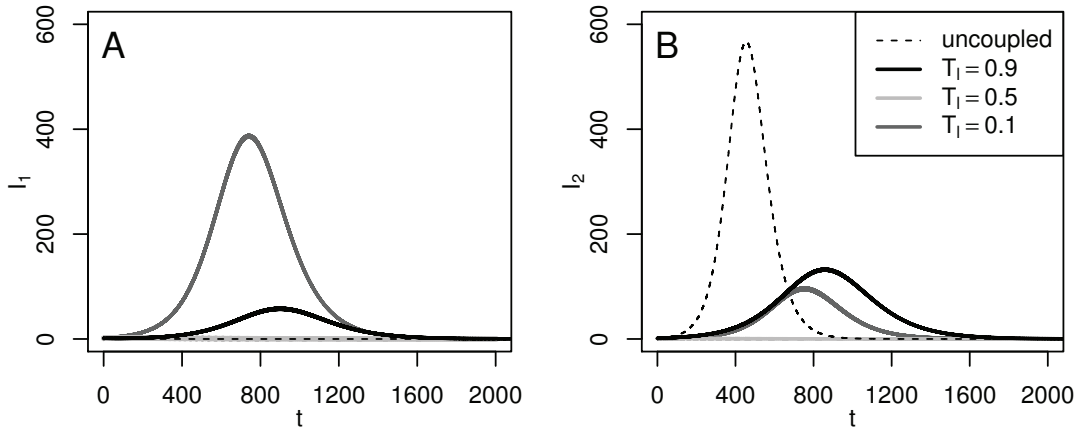

Figure 2.7: Disappearance of outbreaks. Numerical solutions of infected residents (**A**) I_1 and (**B**) I_2, for $N_1^l = 90000$, $N_2^l = 45000$, $\alpha_1 = 0.1$ and $\alpha_2 = 1.0$.

the patches for the existence of an outbreak when patches are uncoupled, there is one due to the human movement. For this, human populations are taken as $N_1^l = N_2^l = 70000$, and $\alpha_1 = 0$ and $\alpha_2 = 0.9$. For uncoupled patches, there are no outbreaks in both patches, which coincides with the fact that both R_{1l} and R_{2l} are smaller than 1 ($R_{1l} = R_{2l} = 0.88$), and, when there is human movement, theoretically $R_{1h} = 0.46$, and $R_{2h} = 8.82$. From Figure 2.8, we observe that an outbreak appears in both patches when $T_l = 0.5$ approximately and becomes longer as the high-activity period increases. In addition, the time in which the outbreak reaches the highest incidence of cases occurs earlier and is larger as T_l decreases. This phenomenon occurs because as the high-activity period increases, the dynamics of patch 2 are governed by $R_{2h} = 8.82$, generating earlier and larger outbreaks in patch 2. For patch 1, in contrast to Figure 2.7, there is an outbreak in patch 1 despite the fact that there are no favorable conditions for the disease development ($R_{1l} = 0.88$ and $R_{1h} = 0.46$). However, as outbreaks appear earlier in patch 2 than in patch 1, those infected individuals from patch 2, who move to patch 1 (90% of individuals), interact with mosquitoes from

patch 1, generating an outbreak in that patch.

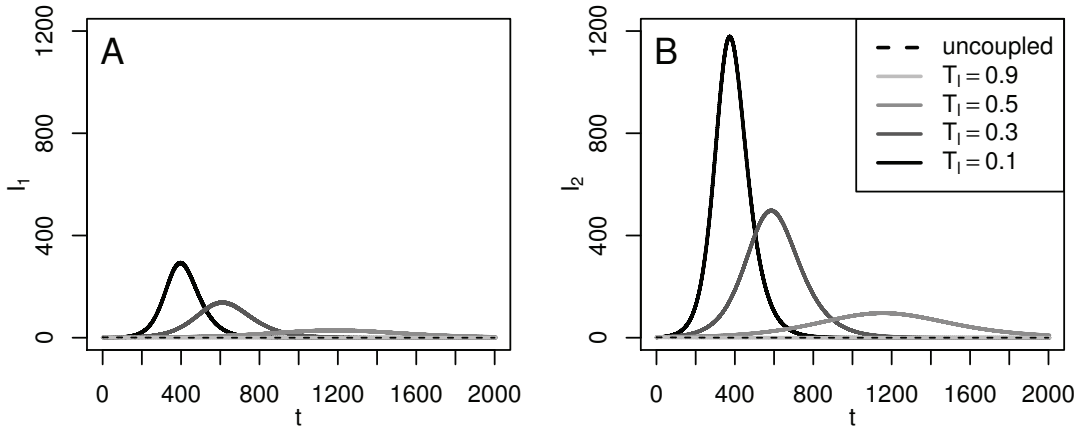

Figure 2.8: Emergence of outbreaks. Numerical solutions of infected residents (**A**) I_1 and (**B**) I_2, for $N_1^l = N_2^l = 70000$, $\alpha_1 = 0$ and $\alpha_2 = 0.9$.

- **Delay and advance of outbreaks**

  To end our study cases, we present scenarios where delay and advance of outbreaks are observed when patches separately have conditions for the existence of outbreaks.

  We first take $N_1^l = 50000$, $N_2^l = 15000$, $\alpha_1 = 0.5$ and $\alpha_2 = 0.1$. For these values, we obtain $R_{1l} = 1.23$, $R_{2l} = 4.11$, $R_{1h} = 2.33$ and $R_{2h} = 1.60$. In Figure 2.9, we notice that if the patches are uncoupled (black dashed lines), the dynamics of both patches are governed by the R_{1l} and R_{2l} values. In this case, the maximum incidence of cases in patch 2 is greater than in patch 1, which coincides with the fact that R_{2l} is much larger than R_{1l}. Compared to the dynamics of the decoupled patches, the outbreaks for $T_l = 0.98$ occur earlier in patch 1, and the one in patch 2 remains practically the same. In this case, the temporal dynamics of the uncoupled system are inherited, that is, although the behavior of the outbreak in patch 1 is preserved, this outbreak is advanced

because patch 2 has a high incidence of cases. As the high-activity period increases, the maximum incidence in patch 1 goes up and the one in patch 2 decreases. In addition, the outbreak in patch 2 is delayed as T_l goes from 0.98 to 0.02. Clearly, these effects are due to $R_{1l} < R_{2l}$ for the low-activity period, but during the high-activity period, the intensity of the basic reproductive numbers is inverted, that is, $R_{1h} > R_{2h}$.

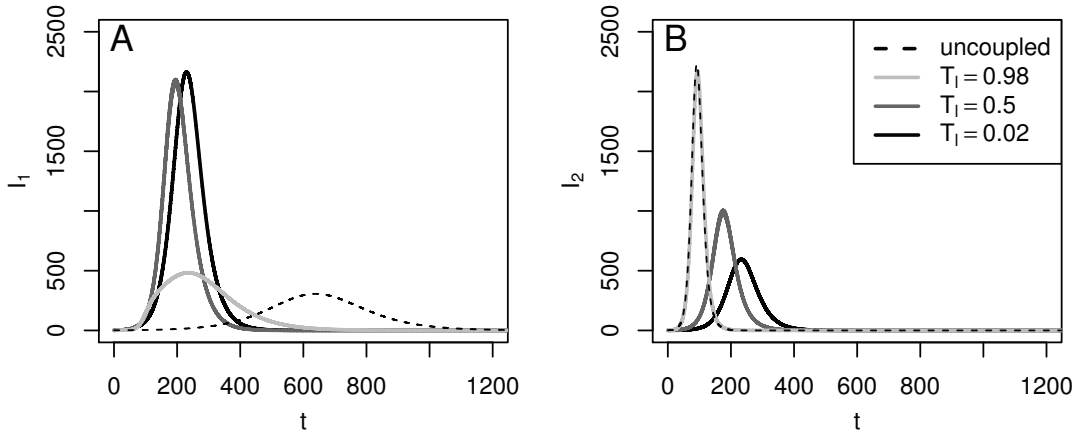

Figure 2.9: Delay and advance of the outbreaks. Numerical solutions of infected residents (**A**) I_1 and (**B**) I_2, for $N_1^l = 50000$, $N_2^l = 15000$, $\alpha_1 = 0.5$ and $\alpha_2 = 0.1$.

Finally, we set $N_1^l = N_2^l = 45000$, $\alpha_1 = 0.2$ and $\alpha_2 = 0.8$. Thus, we have that $R_{1l} = R_{2l} = 1.37$, $R_{1h} = 0.85$ and $R_{2h} = 3.43$. In Figure 2.10, we observe that there are outbreaks when patches are uncoupled (black dashed lines) and these appear earlier when the coupled model is taken into account. Also, the maximum incidence of cases increases as the high-activity period gets longer. In general, this behavior is observed for different settings of α_1 and α_2. To get a better understanding of outbreaks behavior, we analyze how the R_{1h} and R_{2h} values change according to proportions of people who move between patches (α_1 and α_2). In fact, since the conditions of disease spread are identical in both patches, this scenario can be studied directly considering only the difference

between the population that moves from patch 1 to patch 2 and the population that moves from patch 2 to patch 1 (A), defined in Subsection 2.3.2. For this, we assume, without loss of generality, $R_{1h} < R_{2h}$. From Figure 2.11, we have that while R_{1h} decreases, R_{2h} take very large values. In fact, $R_{1h} \in [0.68, 1.37]$, while R_{2h} can be greater than 20. That is, while R_{2h} take values very high and R_{1h} is at least 0.68, the outbreaks appear earlier and the maximum incidence of cases increases.

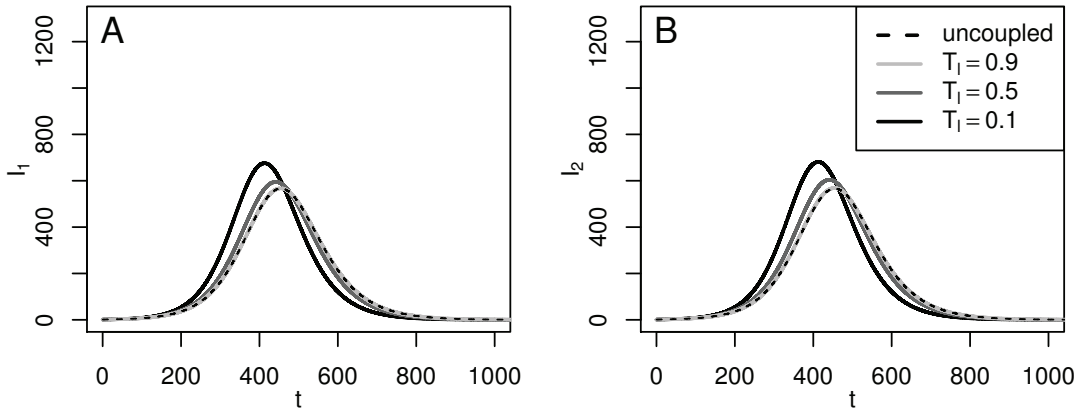

Figure 2.10: Advance of the outbreaks. Numerical solutions for infected residents (**A**) I_1 and (**B**) I_2, for $N_1^l = N_2^l = 45000$, $\alpha_1 = 0.2$ and $\alpha_2 = 0.8$.

2.4 Conclusion and discussion

In this work, our goal was to investigate how the daily human movement affects some characteristics of dengue dynamics based on a two-patch model. The model assumed that the patches are connected by the periodic human movement at discrete times. Given the complexity of the model dynamics, an explicit expression could not be found for the basic reproductive number and the endemic equilibrium points. However, knowing the structure and stability of the equilibrium points and the basic reproductive numbers of the uncoupled system have been useful to determine

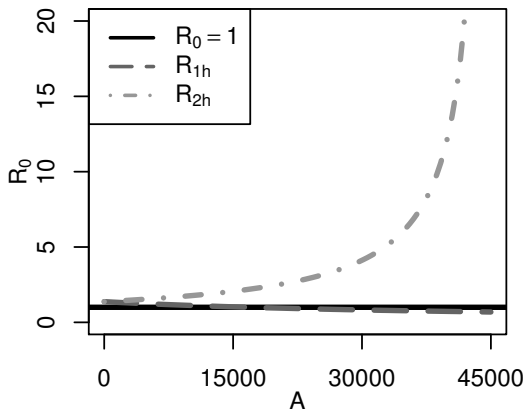

Figure 2.11: Values of R_{1h} and R_{2h} according to the net population that moves between patches (A)

.

when there could be favorable or unfavorable conditions for the existence of endemic equilibrium points and outbreaks for the complete model.

This work studies the effects of daily commuters on the disease dynamics under a little-explored approach, different from traditional multi-patch models. We believe that modeling the spread of infectious diseases, where the division of more than one region is clearly defined, needs to be analyzed with a more complete view. Thus, this approach is helpful for well-defined areas where there is daily human movement between them. Moreover, mixing information from different regions to model it as a single region through a one-patch model without considering movement might give rise to different dynamics than those found in this work. In addition, under this approach, it is possible to recognize where individuals became infected. This fact is important because before applying control measures against possible outbreaks, we should recognize if the cases were imported or autochthonous.

Our scenarios focused on understanding only the effect of human movement on endemic disease levels and on the outbreak dynamics. Some cases of interest were, for example, that although there are regions with disease propagation conditions,

the disease does not necessarily subsist. In addition, there could be regions without favorable conditions for the development of the disease, but human movement might lead to the appearance of outbreaks which is consistent with that reported in [32, 33, 74], where the main carriers of the disease between patches are humans or cattle. However, the advantage of the scenarios presented in this work is that it is possible to have a better biological description of the phenomenon.

From Figures 2.3 to 2.6, the region of disease extinction varies greatly. We have observed that these regions become larger when the basic reproductive numbers of the uncoupled patches are relatively close to 1. Thus, this fact is dependent on the size of interacting populations and the time spent by the populations in their residence patch. These results are not intuitive and might not have been observed unless the movement between two patches is considered. In addition, it is important to mention that although there is no explicit expression for the endemic equilibria points (if any), if a solution tends to an equilibrium point, it will imply that such a point belongs to the system's biological interest. This follows from the results in Appendix 2.A. Therefore, the endemic equilibrium points in Figures 2.3 to 2.6 fall in the system's biological interest region.

Other different scenarios might occur if we assume that the patches have different propagation intensities not related to humans. For example, regions with different sanitary measures or abundant vegetation could lead to different transmission rates, mosquito mortality rate, and mosquito recruitment rate. Thus, table 2.2 could be generalized considering that the parameter values are not the same in both patches. Also, the model can be extended to a network of patches where individuals from each patch spend different high-activity and low-activity periods in neighboring patches. This extended model might give rise to other effects not reported in this work.

Our approach can be useful not only for vector-borne diseases such as zika or chikungunya but also for those with direct transmission such as SARS and COVID-19,

diseases that might generate pandemics due to human movement. In this respect, an infected human might be exposed to different populations during its complete period of infection, leading to a more complex understanding of the basic reproductive number and the disease dynamics. Moreover, to obtain a generalization of the basic reproductive number for our complete model might be useful to establish control policies that consider the human movement.

Finally, we comment on some limitations of the work. The study was mostly computational; however, it was quite complex. This is due to the number of parameters involved in the model dynamics, such as the population sizes of both patches, the proportion of people moving between patches, and the time period individuals spend in their residence patch. Nevertheless, the theoretical behavior for uncoupled patches was essential to provide the information shown in this work. We have also assumed that infected people move between patches without distinguishing between asymptomatic or symptomatic. On the other hand, in most cases, the lengths of the outbreaks given in Figure 2.7 to 2.10 were too long compared to those in the revised literature, which are between 3 months to 1 year [5, 75]. This problem could be due to the absence of seasonality in our model, which controls the presence of disease vectors.

Appendix de Chapter 2

Appendix 2.A Positivity and boundedness of the solution for model (2.2)-(2.3)

In this section, we prove that the solutions of model (2.2)-(2.3) are non-negative and bounded. Since our system (2.2)-(2.3) is piecewise defined in time, we need to know the behavior of the solutions of high-activity and low-activity systems separately. Based on the invariance properties of these systems, we can state the invariance properties of the complete system (2.2)-(2.3). For this, we first prove that any solution of system (2.2) that starts at time $t = t_0$ is non-negative and bounded $\forall t \geq t_0$. Likewise, any solution of system (2.3) that starts at time $t = t_1$ is also non-negative and bounded $\forall t \geq t_1$.

Proposition 1. *The set*

$$\Omega^l = \{(S_1^l, I_1^l, R_1^l, P_1, Q_1, S_2^l, I_2^l, R_2^l, P_2, Q_2) \in \mathbb{R}^{10} : S_i^l \geq 0,\ I_i^l \geq 0,\ R_i^l \geq 0,\ P_i \geq 0,$$
$$Q_i \geq 0,\ S_i^l + I_i^l + R_i^l = N_i^l,\ P_i + Q_i \leq \Lambda_{v_i}/\mu_{vi},\ \textit{for } i, j = 1, 2 \textit{ with } i \neq j\}.$$

is positively invariant for the system of the low-activity period (2.2).

Proof. This proposition follows from the fact that Ω^l is the disjoint union of the positively invariant sets Ω_1 and Ω_2 given in Subsection 2.2.1 for system (2.2) with state variables S_1^l, I_1^l, R_1^l, P_1, and Q_1 ($i = 1$), and with state variables S_2^l, I_2^l, R_2^l, P_2, and Q_2 ($i = 2$), respectively. Therefore, Ω^l is invariant under system (2.2) with state variables S_1^l, I_1^l, R_1^l, P_1, Q_1, S_2^l, I_2^l, R_2^l, P_2, and Q_2.

□

Proposition 2. *The set*

$$\Omega^h = \{(S^h_{11}, I^h_{11}, R^h_{11}, S^h_{21}, I^h_{21}, R^h_{21}, P_1, Q_1, S^h_{22}, I^h_{22}, R^h_{22}, S^h_{12}, I^h_{12}, R^h_{12}, P_2, Q_2) \in \mathbb{R}^{16} :$$
$$S^h_{ii} \geq 0,\ I^h_{ii} \geq 0,\ R^h_{ii} \geq 0,\ S^h_{ij} \geq 0,\ I^h_{ij} \geq 0,\ R^h_{ij} \geq 0,\ P_i \geq 0,\ Q_i \geq 0,$$
$$S^h_{ii} + I^h_{ii} + R^h_{ii} + S^h_{ji} + I^h_{ji} + R^h_{ji} = N^h_i,\ P_i + Q_i \leq \Lambda_{v_i}/\mu_{vi},\ for\ i, j = 1, 2$$
$$with\ i \neq j\}$$

is positively invariant for the system of the high-activity period (2.3).

Proof. This is proven analogously to proposition 1 since system (2.3) can be reduced to system (2.4) given in Subsection 2.2.1. □

Proposition 3. *If propositions 1 and 2 hold, then the solutions of the complete system* (2.2)-(2.3) *are non-negative and bounded.*

Proof. Let $x^{l0}_0 = (S^{l0}_1, I^{l0}_1, R^{l0}_1, P^{l0}_1, Q^{l0}_1, S^{l0}_2, I^{l0}_2, R^{l0}_2, P^{l0}_2, Q^{l0}_2)$ the initial condition for system (2.2) in $t = t_0$ such that $x_0 \in \Omega^l$. From proposition 1, we have that the flow of system (2.2) given by $\Phi^l(x^{l0}_0, t)$ is in Ω^l, $\forall t \geq t_0$ and, in particular, $t \in [t_0, t_1]$. Then, let $x^{h0}_0 = (S^{h0}_{11}, I^{h0}_{11}, R^{h0}_{11}, S^{h0}_{21}, I^{h0}_{21}, R^{h0}_{21}, S^{h0}_{22}, I^{h0}_{22}, R^{h0}_{22}, S^{h0}_{12}, I^{h0}_{12}, R^{h0}_{12}, P^{h0}_1, Q^{h0}_1, P^{h0}_2, Q^{h0}_2)$, where

$$S^{h0}_{11} = (1-\alpha_1)S^l_1(t_1),\ I^{h0}_{11} = (1-\alpha_1)I^l_1(t_1),\ R^{h0}_{11} = (1-\alpha_1)R^l_1(t_1),\ S^{h0}_{21} = \alpha_2 S^l_2(t_1),$$
$$I^{h0}_{21} = \alpha_2 I^l_2(t_1),\ R^{h0}_{21} = \alpha_2 R^l_2(t_1)\ S^{h0}_{22} = (1-\alpha_2)S^l_2(t_1),\ I^{h0}_{22} = (1-\alpha_2)I^l_2(t_1),$$
$$R^{h0}_{22} = (1-\alpha_2)R^l_2(t_1)\ S^{h0}_{12} = \alpha_1 S^l_1(t_1),\ I^{h0}_{12} = \alpha_1 I^l_1(t_1),\ R^{h0}_{12} = \alpha_1 R^l_1(t_1),\ P^{h0}_1 = P_1(t_1),$$
$$Q^{h0}_1 = Q_1(t_1),\ P^{h0}_2 = P_2(t_1),\ Q^{h0}_2 = Q_2(t_1).$$

Since that $(S^l_1(t_1), I^l_1(t_1), R^l_1(t_1), S^l_2(t_1), I^l_2(t_1), R^l_2(t_1), P_1(t_1), Q_1(t_1), P_2(t_1), Q_2(t_1))$

is in Ω^l, then we have that

$$S_{ii}^{h0} \geq 0,\ I_{ii}^{h0} \geq 0,\ R_{ii}^{h0} \geq 0,\ S_{ij}^{h0} \geq 0,\ I_{ij}^{h0} \geq 0,\ R_{ij}^{h0} \geq 0,\ P_i^{h0} \geq 0,\ Q_i^{h0} \geq 0,$$
$$S_{ii}^{h0} + I_{ii}^{h0} + R_{ii}^{h0} + S_{ji}^{h0} + I_{ji}^{h0} + R_{ji}^{h0} = N_i^h,\ P_i^{h0} + Q_i^{h0} \leq \Lambda_{v_i}/\mu_{vi},$$

for $i = 1, 2$, $i \neq j$, which implies that $x_0^{h0} \in \Omega^h$. Then, we take x_0^{h0} as the initial condition for system (2.3) at $t = t_1$. Therefore, from proposition 2, it follows that $\Phi^h(x_0^{h0}, t) \in \Omega^h\ \forall t \geq t_1$ and, in particular, for $t \in [t_1, t_2]$.

Similarly, we define $x_0^{l1} = (S_1^{l1}, I_1^{l1}, R_1^{l1}, P_1^1, Q_1^1, S_2^{l1}, I_2^{l1}, R_2^{l1}, P_2^1, Q_2^1)$, where

$$S_1^{l1} = S_{11}^h(t_2) + S_{12}^h(t_2),\ I_1^{l1} = I_{11}^h(t_2) + I_{12}^h(t_2),\ R_1^{l1} = R_{11}^h(t_2) + R_{12}^h(t_2),\ P_i^{l1} = P_i(t_2),$$
$$S_2^{l1} = S_{22}^h(t_2) + S_{21}^h(t_2),\ I_2^{l1} = I_{22}^h(t_2) + I_{21}^h(t_2),\ R_2^{l1} = R_{22}^h(t_2) + R_{21}^h(t_2),\ Q_i^{l1} = Q_i(t_2).$$

Since that $(S_{11}^h(t_2), I_{11}^h(t_2), R_{11}^h(t_2), S_{21}^h(t_2), I_{21}^h(t_2), R_{21}^h(t_2), S_{22}^h(t_2), I_{22}^h(t_2), R_{22}^h(t_2), S_{12}^h(t_2), I_{12}^h(t_2), R_{12}^h(t_2), P_1^h(t_2), Q_1^h(t_2), P_2^h(t_2), Q_2^h(t_2)) \in \Omega^h$, then we have that

$$S_i^{l1} \geq 0,\ I_i^{l1} \geq 0,\ R_i^{l1} \geq 0,\ P_i^{l1} \geq 0,\ Q_i^{l1} \geq 0,$$
$$S_i^{l1} + I_i^{l1} + R_i^{l1} = N_i^l,\ P_i^{l1} + Q_i^{l1} \leq \Lambda_{v_i}/\mu_{vi},$$

for $i = 1, 2$, $i \neq j$, which implies that $x_0^{l1} \in \Omega^l$. Then, we have x_0^{l1} as the initial condition for system (2.2) at $t = t_2$. Therefore, we have proved that solutions that start in Ω^l are sent to values inside Ω^h at the switching times. These values are initial conditions in Ω^h, which in turn will generate solutions that are sent back to values in Ω^l, and therefore, repeating the whole process, we obtain that solutions for system (2.2)-(2.3) are non-negative and bounded where the upper bound is given by each of the bounds of Ω^l and Ω^h. □

Appendix 2.B Deduction of conditions given in Table 2.2

Here we deduce the conditions for scenarios (a) to (d) for case $R_{1l} < 1$ and $R_{2l} > 1$.

For case (1), we have $R_{1l} < 1$ and $R_{2l} > 1$ which implies $N_1^l > \overline{N}$ and $N_2^l < \overline{N}$. We now look for conditions such that

(a) $R_{1h} < 1$ and $R_{2h} < 1$ ($N_1^h > \overline{N}$ and $N_2^h > \overline{N}$),

(b) $R_{1h} < 1$ and $R_{2h} > 1$ ($N_1^h > \overline{N}$ and $N_2^h < \overline{N}$),

(c) $R_{1h} > 1$ and $R_{2h} < 1$ ($N_1^h < \overline{N}$ and $N_2^h > \overline{N}$),

(d) $R_{1h} > 1$ and $R_{2h} > 1$ ($N_1^h < \overline{N}$ and $N_2^h < \overline{N}$),

holds. From the definition of A, N_1^h and N_2^h, we have

$$N_1^h = N_1^l - A,$$
$$N_2^h = N_2^l + A.$$

We now proceed to find the conditions for N_1^h and N_2^h.

Case (a): We look for conditions in A such that $N_1^h > \overline{N}$ and $N_2^h > \overline{N}$ holds. This follows if $N_1^l - A > \overline{N}$ and $N_2^l + A > \overline{N}$. Therefore, we need $\overline{N} - N_2^l < A < N_1^l - \overline{N}$ to have our statement.

Case (b): In this case we look for conditions in A such that $N_1^h > \overline{N}$ and $N_2^h < \overline{N}$ holds. This follows if $N_1^l - A > \overline{N}$ and $N_2^l + A < \overline{N}$. Then, we need $A < N_1^l - \overline{N}$ and $A < \overline{N} - N_2^l$ which implies $A < \min\left\{N_1^l - \overline{N}, \overline{N} - N_2^l\right\}$.

Case (c): Here we look for conditions in A such that $N_1^h < \overline{N}$ and $N_2^h > \overline{N}$. This follows if $N_1^l - A < \overline{N}$ and $N_2^l + A > \overline{N}$ which implies that $A > N_1^l - \overline{N}$ and $A > \overline{N} - N_2^l$. Then, we need $A > \max\left\{N_1^l - \overline{N}, \overline{N} - N_2^l\right\}$ to have our statement.

Case (d): In this case we look for $N_1^h < \bar{N}$ and $N_2^h < \overline{N}$. This follows if $N_1^l - A < \overline{N}$ and $N_2^l + A < \overline{N}$. Then, we need $A > N_1^l - \overline{N}$ and $A < \overline{N} - N_2^l$ which implies that $N_1^l - \overline{N} < A < \overline{N} - N_2^l$ to have our statement. Note that this range of values for A will be empty if Case (a) holds.

Chapter 3

Effect of daily periodic human movement on dengue dynamics: The case of the 2010 outbreak in Hermosillo, Mexico*

3.1 Introduction

An important factor in the spread of infectious diseases as dengue is the human movement [68]. Due to this fact, dengue can be expanded from endemic to non-endemic places [70]. It has been suggested that infectious diseases may persist in a region where transmission rates are very low due to interaction with people from other areas with high transmission rates [25]. On an urban scale, daily movement occurs motivated by commuting people to workplaces, schools, commerce, among others [13].

Human mobility has been included in the latest generation of models in epidemiology using two main approaches: agent-based modeling and metapopulations [76]. Metapopulation models divide the population into interacting population groups defined by spatial or demographic information [77]. This mathematical modeling approach, based on ordinary differential equations, has been used to theoretically evaluate the effect of human mobility on the dynamics of infectious diseases in

*This article was published in Applied Mathematical Modelling, Vol. 97, Mayra R. Tocto-Erazo, Daniel Olmos-Liceaga and José A. Montoya-Laos, Effect of daily periodic human movement on dengue dynamics: The case of the 2010 outbreak in Hermosillo, Mexico, 559-567, Copyright Elsevier (2021).

heterogeneous regions connected by mobility [25, 31–34, 78]. The consequences of mobility between cities have been analyzed in [27, 75, 79], whereas between an urban and suburban regions in [35, 36, 80], or between areas within the same city in [81]. There are some efforts to use real data to validate the effect of human movement, but there are few studies yet [35, 75, 81]. Authors in [75, 81] have concluded that infectious diseases could spread in disease-free areas or with a local basic reproductive number less than one due to the human movement. In particular, authors in [75] study different factors for the transmission of dengue disease in a Chinese province using a residence time approach. They analyze the human movement between seven regions, estimate model parameters for each patch based on a fixed residence time matrix and explore some hypothetical scenarios by reducing the values of such matrix.

Similar to [75], we are interested in studying the daily human mobility between two regions from an urban area to explore how the transmission rates and the local basic reproductive numbers may vary depending on the time period of daily local stay of a population within their residence place. For this, we use a two-patch mathematical model under a little-explored approach [36, 40] and data from the 2010 dengue outbreak in Hermosillo, Mexico. We used the ideas of a previous work [40] and applied them to a scenario where the commutation between patches emerges naturally. To define each of two patchs of the model, we divide Hermosillo into two regions, which was derived from a preliminary cluster analysis. Finally, we use a Bayesian approach to estimate some parameters of the model and compare mobility scenarios.

This work is divided into the following sections. The description of the model used, the data, and the inference method are given in Section 3.2. Then, in Section 3.3, we show the estimation results. Finally, the conclusions and discussions on our results are presented in Section 3.4.

3.2 Methods

3.2.1 Mathematical model

We consider a previous two-patch model without vital dynamics in humans and daily human movement, where movement ocurs at periodic discrete times [40]. Here the interval $[t_k, t_{k+1})$ represent the kth day and is divided into two time periods: low-activity period $[t_k, t_k + T_l)$ and high-activity period $[t_k + T_l, t_{k+1})$, where T_l represents the fraction of the kth day of low activity and $T_l \in (0, 1)$. The daily dynamics between the periods of low-activity and high-activity are as follows. At the beginning of high-activity periods, people move to the other patch to carry out their daily activities. Then, at the end of high-activity periods, people return to their residence patch and stay there during the low-activity periods.

The following equations represent the dynamics of the populations for the low-activity period $[t_k, t_k + T_l)$:

$$\begin{aligned}
\dot{S}_i^l(t) &= -\frac{\alpha_{hi} S_i^l(t) Q_i(t)}{N_{il}}, \\
\dot{I}_i^l(t) &= \frac{\alpha_{hi} S_i^l(t) Q_i(t)}{N_{il}} - \gamma_i I_i^l(t), \\
\dot{R}_i^l(t) &= \gamma_i I_i^l(t), \\
\dot{P}_i(t) &= \mu_{vi} M_i - \frac{\alpha_{vi} P_i(t) I_i^l(t)}{N_{il}} - \mu_{vi} P_i(t), \\
\dot{Q}_i(t) &= \frac{\alpha_{vi} P_i(t) I_i^l(t)}{N_{il}} - \mu_{vi} Q_i(t),
\end{aligned} \tag{3.1}$$

where $N_{il} := N_i$ and $i = 1, 2$.

For the high-activity period $[t_k + T_l, t_{k+1})$, the set of equations become:

$$
\begin{aligned}
\dot{S}^h_{ii}(t) &= -\frac{\alpha_{hi} S^h_{ii}(t) Q_i(t)}{N_{ih}},\\
\dot{I}^h_{ii}(t) &= \frac{\alpha_{hi} S^h_{ii}(t) Q_i(t)}{N_{ih}} - \gamma_i I^h_{ii}(t),\\
\dot{R}^h_{ii}(t) &= \gamma_i I^h_{ii}(t),\\
\dot{S}^h_{ji}(t) &= -\frac{\alpha_{hi} S^h_{ji}(t) Q_i(t)}{N_{ih}},\\
\dot{I}^h_{ji}(t) &= \frac{\alpha_{hi} S^h_{ji}(t) Q_i(t)}{N_{ih}} - \gamma_i I^h_{ji}(t),\\
\dot{R}^h_{ji}(t) &= \gamma_i I^h_{ji}(t),\\
\dot{P}_i(t) &= \mu_{vi} M_i - \frac{\alpha_{vi} P_i(t)(I^h_{ii}(t) + I^h_{ji}(t))}{N_{ih}} - \mu_{vi} P_i(t),\\
\dot{Q}_i(t) &= \frac{\alpha_{vi} P_i(t)(I^h_{ii}(t) + I^h_{ji}(t))}{N_{ih}} - \mu_{vi} Q_i(t),
\end{aligned}
\tag{3.2}
$$

where $N_{ih} := (1-\alpha_i)N_i + \alpha_j N_j$, and $i, j = 1, 2, i \neq j$. All model parameters and meaning of the state variables are defined in Table 3.1.

We assume that the infected classes both I^h_{12} and I^h_{21}, who move between patches, represent only individuals with mild or no symptoms. On the other hand, uncoupled case ($T_l = 1$) is obtained considering $\alpha_1 = \alpha_2 = 0$ in model (3.1)-(3.2). That is, system (3.1)-(3.2) is reduced to the dynamics of a vector-host model as in (3.1) for all time t.

Using the next generation matrix approach as in [72], the basic reproductive number (R_{0i}) of the uncoupled case is given by

$$
R_{0i} := \frac{\alpha_{hi}\alpha_{v_i}\rho_i}{\mu_{v_i}\gamma_i}, \tag{3.3}
$$

where $\rho_i = M_i/N_i$. Given the complexity of the model, the basic reproductive number for model (3.1)-(3.2) was not found. However, R_{01} and R_{02} can give us an approximation of a local indicator of the severity of the disease for both the uncoupled and the coupled cases.

Variable or parameter	Definition
N_i	Total population from patch i.
N_{ih}	Total population in patch i during the high-activity period.
M_i	Total population of mosquitoes from patch i.
S_i^l	Susceptible residents from patch i.
I_i^l	Infected residents from patch i.
R_i^l	Recovered residents from patch i.
S_{ii}^h	Susceptible residents from patch i who do not commute to another patch during the low-activity period.
I_{ii}^h	Infected residents from patch i who do not commute to another patch during the low-activity period.
R_{ii}^h	Recovered residents from patch i who do not commute to another patch during the low-activity period.
S_{ji}^h	Susceptible residents from patch j who commute to patch i during the high-activity period.
I_{ji}^h	Infected residents from patch j who commute to patch i during the high-activity period.
R_{ji}^h	Recovered residents from patch j who commute to patch i during the high-activity period.
P_i	Susceptible vector population.
Q_i	Infected vector population.
α_{hi}	Transmission rate from mosquito to human in patch i.
α_{vi}	Transmission rate from human to mosquito in patch i.
$1/\gamma_i$	Average recovery time of humans in patch i.
$1/\mu_{vi}$	Average lifetime of mosquitoes in patch i.
α_i	Proportion of humans from patch i who move to patch j at time $t_k + T_l$.

Table 3.1: Variable and parameter definition of model (3.1)-(3.2).

3.2.2 Data

Hermosillo is a city located in the north of Mexico, with a total population of 715061 inhabitants according to the 2010 Census data provided by the National Institute of Statistics, Geography and Informatics from Mexico (INEGI). To divide the city of Hermosillo into two regions, we group the AGEBs using a hierarchical cluster

analysis and a Geographic Information System (GIS). We construct the economically active population density variable using data from the 2010 census given by INEGI. According to the cluster analysis, we observe that most of the AGEBs in the north of the city belong to the same group. Based on this, we divided the city into two regions: north and south side (see Figure 3.1). The north side has 374102 inhabitants and the south side 340959. On the south side are located the municipal and state government offices, the city center, the largest university, and industrial parks, among others. Thus, we consider that the flow from north to south of the city is greater than from south to north.

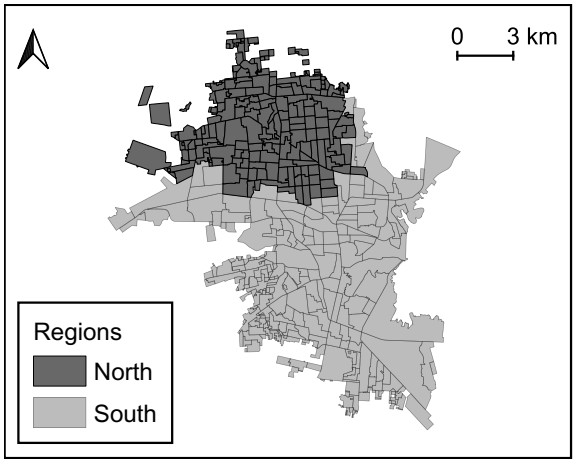

Figure 3.1: Geographical division of Hermosillo in two regions: north (dark gray) and south (light gray).

According to data provided by the Health Ministry of the State of Sonora, 2139 dengue cases were located on the north aloneng 52 epidemiological weeks resulting in a rate of 57.17 cases/10000 inhabitants, and 590 dengue cases in the south with a rate of 17.3 cases/10000 inhabitants during 2010. In this study, we use the weekly incidence from epidemiological week 33 to 40 for both regions north and south from Hermosillo.

3.2.3 Mobility scenarios

According to information from the 2010 census by INEGI, the economically active population of the north side is approximately 45%. Moreover, as mentioned above, workplaces of the city are mostly located on the south side. Therefore, we assume that all that 45% of economically active people from the north side ($\alpha_1 = 0.45$) moves to the south side during the high-activity period, while we establish that only 10% of the resident population from the south side ($\alpha_2 = 0.1$) moves to the north side.

On the other hand, to represent that the time people spend daily on another patch is 6 and 12 hours, we take $T_l = 0.75$ and $T_l = 0.5$, respectively. In addition, because our objective is to explore the effect of daily local stay on some characteristics of the dynamics, $T_l = 1$ was selected, which allowed us to compare the scenario without mobility versus with mobility ($T_l < 1$).

3.2.4 Parameter estimation

We first add a class C_i ($i = 1, 2$) to system (3.1)-(3.2), which represents the accumulated number of reported infected residents from patch i, and is given by

$$\dot{C}_i(t) = \begin{cases} \delta \times \frac{\alpha_{hi} S_i^l(t) Q_i(t)}{N_{il}} & \text{if } t_k \leq t < t_k + T_l \\ \delta \times \frac{\alpha_{hi} S_{ii}^h(t) Q_i(t)}{N_{ih}} + \delta \times \frac{\alpha_{hj} S_{ij}^h(t) Q_j(t)}{N_{jh}} & \text{if si } t_k + T_l \leq t < t_{k+1} \end{cases} \tag{3.4}$$

where $i \neq j$ ($j = 1, 2$), and δ represents the proportion of infected individuals confirmed by the surveillance system of the state government of Sonora. The new parameter (δ) will be estimated. Equation (3.4) will calculate the number of new weekly cases.

For our estimation process, we have taken values for the parameter model inside the reported range in Table 3.2. We take the average lifetime of mosquitoes ($1/\mu_{vi}$, $i = 1, 2$) as two weeks and the number of mosquitoes per person equal to 2. For

each T_l fixed value (1, 0.75 and 0.5) with $\alpha_1 = 0.45$ and $\alpha_2 = 0.1$, we use the data to estimate the remaining seven parameters ($\alpha_{h1}, \gamma_1, \alpha_{v2}, \alpha_{h2}, \gamma_2, \alpha_{v2},$ and δ) by Bayesian inference approach.

Parameter	Value or range
$1/\mu_{v1}$, $1/\mu_{v2}$ (days)	$4-50$ [59]
ρ	$1-10$ [82]
δ	0.08 [83]
α_{h1}, α_{h2}	$0.03-0.75$ [59]
α_{v1}, α_{v2}	$0.15-1$ [59]
$1/\gamma_1, 1/\gamma_2$ (days)	$3-7$ [58]

Table 3.2: Parameter source.

Similar to Chapter 1, we take logarithmic transformations as

$$\tilde{\alpha}_{h1} = \log(\alpha_{h1}), \qquad \tilde{\gamma}_1 = \log(\gamma_1), \qquad \tilde{\alpha}_{v1} = \log(\alpha_{v1}), \tag{3.5}$$

$$\tilde{\alpha}_{h1} = \log(\alpha_{h1}), \qquad \tilde{\gamma}_1 = \log(\gamma_1), \qquad \tilde{\alpha}_{v1} = \log(\alpha_{v1}). \tag{3.6}$$

Thus, we assign a normal distribution to the six parameters given in (3.5)-(3.6). We take a mean equal to $\log(0.3)$ and a standard deviation of 0.4 for the distribution of $\tilde{\alpha}_{h1}$ and $\tilde{\alpha}_{h2}$, a mean equal to $\log(0.22)$ and a standard deviation of 0.1 for the distribution of $\tilde{\gamma}_1$ and $\tilde{\gamma}_2$, and a mean equal to $\log(0.4)$ and a standard deviation of 0.3 for the distribution of $\tilde{\alpha}_{v1}$ and $\tilde{\alpha}_{v2}$. On the other hand, given that the support of the beta distribution is $[0, 1]$ and its known versatility to assign a greater or lower probability density to values of interest, we assign a priori beta distribution for δ with shape parameters $\alpha = 5$ and $\beta = 50$. To establish the mean and standard deviation of the normal distributions for parameters (3.5)-(3.6) and shape parameters for δ, we considered the values or ranges given in Table 3.2. Therefore, the prior joint density function of $(\tilde{\alpha}_{h1}, \tilde{\gamma}_1, \tilde{\alpha}_{v1}, \tilde{\alpha}_{h2}, \tilde{\gamma}_2, \tilde{\alpha}_{v2}, \delta)$ is given by

$$\pi(\tilde{\alpha}_{h1}, \tilde{\gamma}_1, \tilde{\alpha}_{v1}, \tilde{\alpha}_{h2}, \tilde{\gamma}_2, \tilde{\alpha}_{v2}, \delta) = \pi(\tilde{\alpha}_{h1})\pi(\tilde{\gamma}_1)\pi(\tilde{\alpha}_{v1})\pi(\tilde{\alpha}_{h2})\pi(\tilde{\gamma}_1)\pi(\tilde{\alpha}_{v2})\pi(\delta), \tag{3.7}$$

where $\pi(\bullet)$ is the normal density function of each parameter defined above.

Since model (3.1)-(3.2) is in a time-scale of days and starts at $t = 0$, we define D_w^i to represent the number of new infectious cases of dengue at wth week ($w = 33, ..., 40$) in patch i, which is given by

$$D_{32+k}^i = \int_{7k}^{7k-7} \dot{C}_i(t)dt,$$

where $k = 1, 2, ..., 8$, and $C_i(j)$ defined as (3.4). We define patch 1 as the north area and patch 2 as the south area. Thus, we consider that the new weekly cases at week w from patch 1 and patch 2 follow a Poisson distribution with a mean $\lambda_w^1(\theta) = D_w^1$ and $\lambda_w^2(\theta) = D_w^2$, respectively, where $\theta = (\tilde{\alpha}_{h1}, \tilde{\gamma}_1, \tilde{\alpha}_{v1}, \tilde{\alpha}_{h2}, \tilde{\gamma}_2, \tilde{\alpha}_{v2}, \delta)$. Thus, the sampling distribution is given by

$$\pi\left(\vec{x}|\theta\right) = \prod_{w=33}^{40} \frac{1}{x_w^1!} \left[\lambda_w^1\left(\theta\right)\right]^{x_w^1} \exp\left[-\lambda_w^1\left(\theta\right)\right] \prod_{w=33}^{40} \frac{1}{x_w^2!} \left[\lambda_w^2\left(\theta\right)\right]^{x_w^2} \exp\left[-\lambda_w^2\left(\theta\right)\right], \tag{3.8}$$

where $(x_{33}^i, x_{34}^i, ..., x_{40}^i)$ is the observed data from patch i, and $\vec{x} = (x_{33}^1, x_{34}^1, ..., x_{40}^1,$ $x_{33}^2, x_{34}^2, ..., x_{40}^2)$. Therefore, the posterior distribution $\pi(\theta|\vec{x})$ is given by

$$\pi(\theta|\vec{x}) \propto \pi\left(\vec{x}|\theta\right)\pi(\theta),$$

where $\pi(\theta)$ and $\pi\left(\vec{x}|\theta\right)$ are given in (3.7) and (3.8), respectively.

To obtain the estimated probability density of the model parameters, we used an MCMC method based on the Metropolis-Hasting algorithm [60]. We run the algorithm for 200000 iterations but we use the last 50000 to generate the posterior densities of the parameters and the posterior predictive distributions to check the fit. The initial conditions assumed are as follows: $S_1^l(0) = N_1 - 1$, $I_1^l(0) = 1$, $R_1^l(0) = 0$, $P_1(0) = \rho N_1$, $Q_1(0) = 0$, $S_2^l(0) = N_2 - 1$, $I_2^l(0) = 1$, $R_2^l(0) = 0$, $P_2(0) = \rho N_2$, and $Q_2(0) = 0$, where $N_1 = 374102$ and $N_2 = 340959$. To generate the posterior density of

R_{01} and R_{02}, we replace each sample of $(\alpha_{h1}, \gamma_1, \alpha_{v1}, \alpha_{h2}, \gamma_2, \alpha_{v2}, \delta)$ in equation (3.3). The code used to calculate the posterior predictive distribution is available online at https://github.com/MayraTocto/DailyHumanMobility_DengueOutbreak.

3.3 Results

The results are based on three scenarios: $T_l = 1$, $T_l = 0.75$, and $T_l = 0.5$. Case $T_l = 1$ represents that there is no flow of people between the north and south regions. Cases $T_l = 0.75$ and $T_l = 0.5$ indicate that the residents from each patch spend 75% and 50% of their day at their residence place, respectively. To check the fit of the model to the data, we construct 95% predictive intervals of the posterior predictive distributions using the 0.025 and 0.975 quantiles for the north and south sides, as shown in Figure 3.2. This figure shows that the three scenarios are plausible. In the following lines, we will see some differences in the estimates of the model parameters, which implies that the local basic reproductive numbers may drastically change.

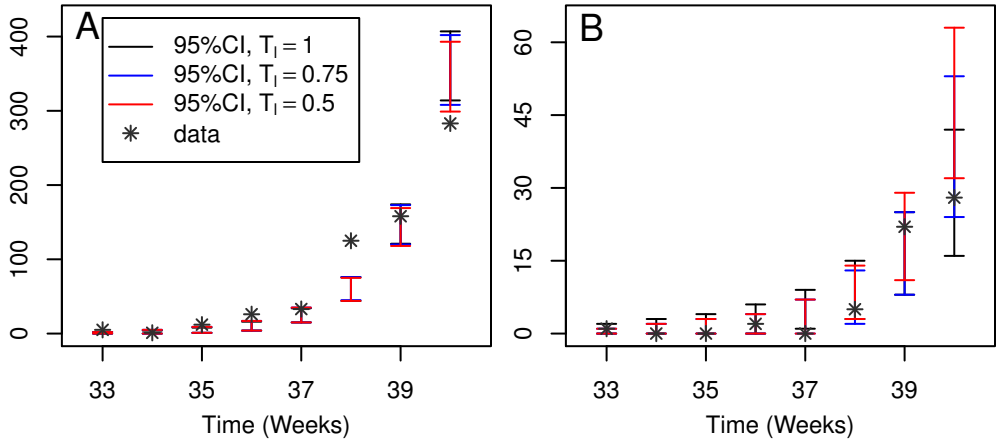

Figure 3.2: The 95% predictive intervals for the estimated posterior predictive distributions from the north side (**A**) and south side (**B**) versus data from dengue cases in Hermosillo.

Figure 3.3 shows the posterior densities of transmission rates for the north and

south regions. The range of most likely values for estimated local transmission rates from the north side (α_{h1} and α_{v1}) coincides for $T_l = 1$, $T_l = 0.75$, and $T_l = 0.5$ (Figure 3.3A and 3.3B). Based on our mobility scenarios, this fact could indicate that the daily mobility of people does not affect the disease dynamics on the north side of the city. On the contrary, the posterior density for local transmission rates (α_{h2} and α_{v2}) from the south region, when $T_l < 1$, has more weight in lower values compared to the case $T_l = 1$ (Figure 3.3C and 3.3D). That is, it would be more likely to obtain smaller values for the transmission rates on the south side when T_l goes down from 1 to 0.5, and, therefore, local contagions decrease. In this case, according to the T_l value ($T_l < 1$), infected individuals from the south side who get the dengue virus during their visit to the north side is more credible than local contagions. Thus, the results may suggest that some dengue cases from the south side may have emerged by the interaction between a susceptible individual from the south side that gets bitten by an infected mosquito from the north of the city during his visit. The median and 95% confidence intervals of the posterior distributions for γ_1, γ_2, and δ are given in Table 3.3.

Parameter	**Median (95% CI) for $T_l = 1$**	**Median (95% CI) for $T_l = 0.75$**	**Median (95% CI) for $T_l = 0.5$**
γ_1	0.250 ([0.206, 0.305])	0.252 ([0.207, 0.307])	0.253 ([0.208, 0.309])
γ_2	0.230 ([0.189, 0.280])	0.231 ([0.192, 0.283])	0.233 ([0.192, 0.284])
δ	0.429 ([0.337, 0.526])	0.436 ([0.344, 0.530])	0.436 ([0.342, 0.532])

Table 3.3: Estimation of γ_1, γ_2, and δ parameters.

Based on the samples obtained for the parameters and replacing them in expression (3.3), we obtain the estimated density of local basic reproductive numbers (for $T_l = 1$, $T_l = 0.75$, and $T_l = 0.5$). As we have already mentioned, for $T_l < 1$, the local basic reproductive number is used as a local indicator of the disease, that is, these values would tell us how severe could be the disease locally. Figure 3.4 shows the posterior

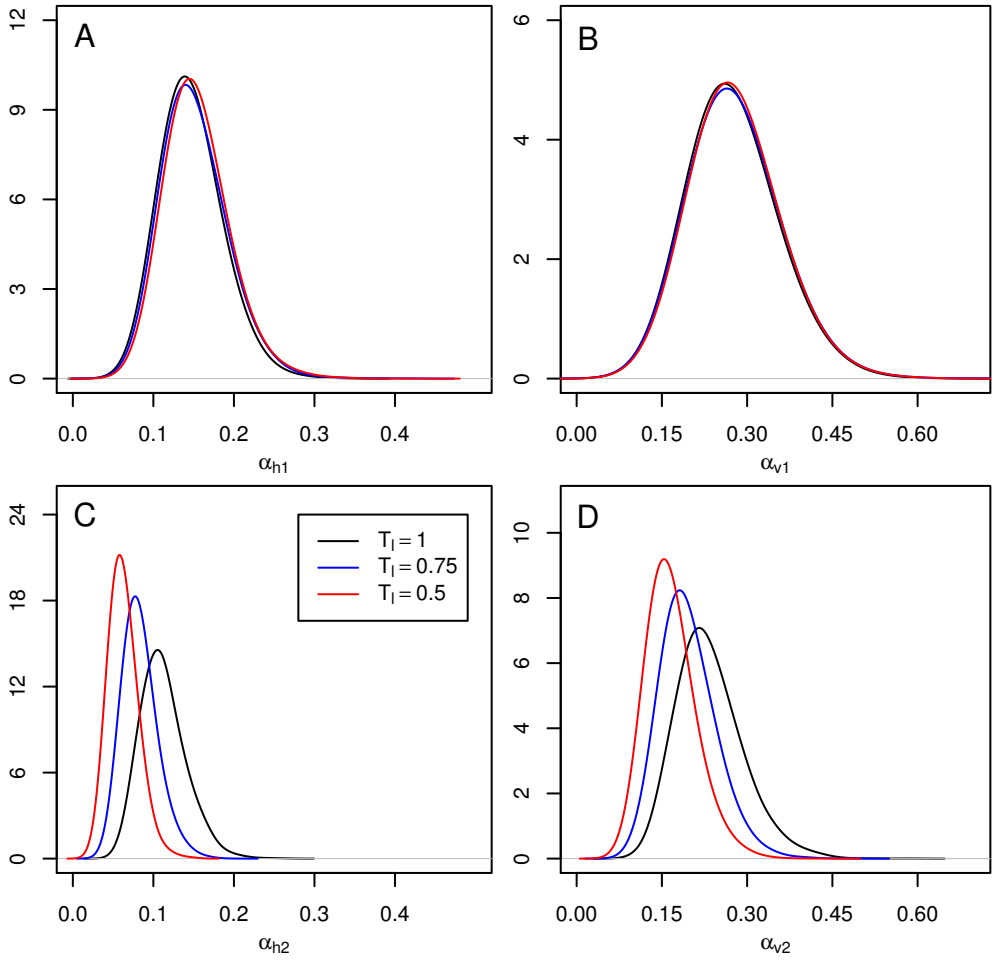

Figure 3.3: The posterior density of parameters from the north patch (**A** and **B**) and south patch (**C** and **D**).

densities of R_{01} and R_{02}. From Figure 3.4A, we have that R_{01} is more likely to take values greater than 1 for all three cases. However, if we consider $T_l = 0.75$, we have that the most probable values for R_{02} are smaller compared to the case $T_l = 1$ as we can see in Figure 3.4B. Furthermore, if $T_l = 0.5$, the probability that R_{02} takes on values less than 1 is not negligible.

The estimates obtained above coincides with the fact that there was only 1 confirmed case of dengue on the south side from 33th to 35th week, while on the

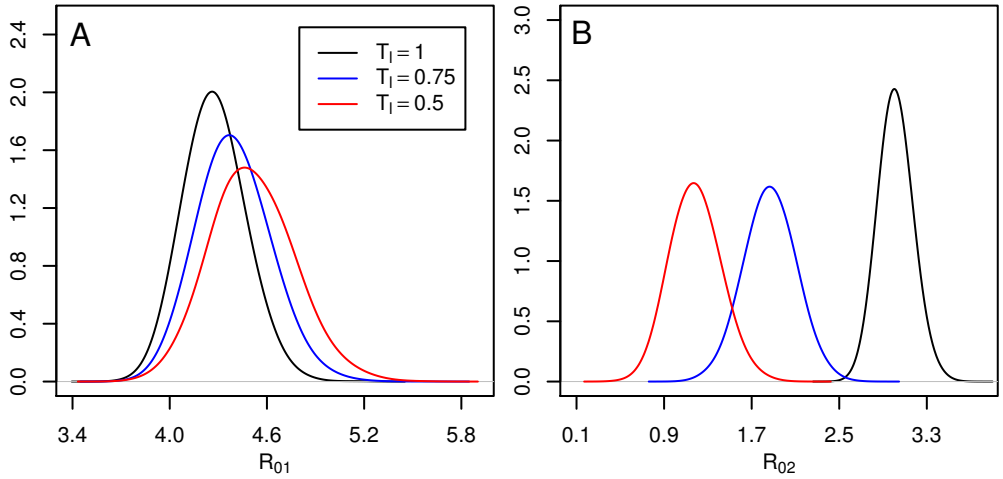

Figure 3.4: The posterior density of R_0 from the north side (A) and the south side (B).

north side there were 18 cases in the same period of time, see Figure 3.2. Thus, the appearance of a dengue outbreak in the south region may be due to the daily movement of people. These results may suggest that not considering daily human movement overestimates the transmission rates and the local basic reproductive number of the south side of the city. The daily mobility between both patches decreased the estimated values of the local transmission rates of the South side, attributing the outbreak on that side due to the connection with the North side.

3.4 Conclusions and discussions

Many mathematical models based on ordinary differential equations have been used to model infectious disease dynamics throughout a country or a city. We believe it is essential to consider that an area may have, for example, different demographic and socio-economic characteristics which may be affected by the daily mobility of people. Considering these factors for modeling the disease dynamics and estimating the model parameter are very important because they take into account heterogeneities within

a region and provides a way to analyze possible effects on each local dynamics of the disease.

Here we have explored a scenario of human mobility by fitting data of a dengue outbreak from Hermosillo to a two-patch mathematical model. For the estimation process, we have only used data from the initial stage of the outbreak because many factors can influence the disease dynamics for the complete outbreak. In addition, since no data are available on the mosquito population, some assumptions based on literature were made for parameters related to the vector. On the other hand, despite not having an overall R_0 of coupled model (3.1)-(3.2), the expression for the basic reproductive number given in (3.3) was helpful to measure the local severity of the disease in each patch.

Based on the results, we have observed that not considering the daily mobility between connected areas may lead to inappropriate conclusions of some characteristics of the disease dynamics. For example, we have obtained higher estimates of transmission rates and local basic reproductive numbers on the south side if it is assumed that there is no flow of people between the north and south sides of the city. This fact could lead to suppose that the conditions for the spread of the disease on the south side may be relatively similar to the north side. However, the results may suggest that some infected residents of the south side could be a contribution of daily mobility, but not because of the conditions on that side of the city, which is consistent with previous results [68, 75, 81]. The latter could lead to more appropriate decisions regarding where to focus the control measures when an outbreak is stronger. Thus, despite having a reasonable fit of the uncoupled model to the data (case $T_l = 1$), we must consider the role of human mobility and how this could significantly affect the dynamics in regions without conditions of disease development. Similar conclusions were obtained for other settings of the proportions that move between patches (α_1 and α_2, with $\alpha_1 > \alpha_2$).

This work is supported by the available data of dengue cases within a population and a socio-economic and socio-demographic analysis to study the city as two regions connected by the human movement. However, in general, we could better understand the local properties of a community if we had more documented information about mobility. This latter could help to detect contagion risk areas within the same community.

The current problem was addressed initially to study vector-borne infectious diseases, where the vector has much more limited mobility than hosts (humans). However, this approach can be applied to infectious diseases with human-to-human transmission via direct contact. The COVID-19 pandemic is a clear example that the human movement represents a critical factor in the spread of infectious diseases. In this sense, this mobility approach can be used to analyze situations where the human movement has a periodic nature. Examples of this idea are schools, workplaces, or even large events that last more than one day. Multiple connected patches can also be considered under this same approach. These types of studies allow analyzing the weight of commuters in the disease dynamics, which may be useful to propose control policies and reduce cases or prevent outbreaks in certain city locations.

Finally, in this work, we have assumed that the length of the high-activity periods is the same each day. However, not only may this length change on weekends, but also the start and end of high-activity periods may vary. We also can consider the peak biting periods of mosquitoes: early in the morning and in the evening before dusk [4]. These types of differentiated mobility behaviors will follow from this study. We consider the present work as a starting point to address these new mobility scenarios.

Chapter 4

A Monte Carlo study for COVID-19 in Hermosillo*

On March 16, 2020, the state government of Sonora declared mandatory confinement for the COVID-19 pandemic. Given this, at the request of the state authorities, the biomathematics team of the University of Sonora proposed a mathematical model to explore Covid-19 spread scenarios in Sonora [38]. As a consequence of work done by the biomathematics team, the author of this manuscript was invited to participate in the team to explore some characteristics of COVID-19 dynamics in Hermosillo, such as the acme value and acme date, and to compare the implemented measures with other hypothetical scenarios such as the delay of one or two weeks of the start date of the lockdown. In this sense, a methodology based on a Montecarlo method was proposed joined with Dr. José Arturo Montoya Laos and MSc. Jorge Alberto Espíndola Zepeda.

Next, we present the methodology and results according to a scenario proposed by the author of this manuscript for the COVID-19 dynamic in Hermosillo.

*Most of the material presented in this chapter was published in PLoS ONE journal, Vol. 97, Mayra R. Tocto-Erazo, Jorge A. Espíndola-Zepeda, José A. Montoya-Laos, Manuel A. Acuña-Zegarra, Daniel Olmos-Liceaga, Pablo A. Reyes-Castro, and Gudelia Figueroa-Preciado, Lockdown, relaxation, and acme period in COVID-19: A study of disease dynamics in Hermosillo, Sonora, Mexico, e0242957 (2020).

4.1 Montecarlo study

We will first present the mathematical model used, and then we will provide the steps to apply the Monte Carlo method.

4.1.1 Mathematical model

The mathematical model is an extension of the SIR model that considers the following classes: susceptible (S), exposed (E), asymptomatic infectious (I_A), symptomatic infectious (I_S), recovered (R), quarantined (Q), hospitalized (H), dead individuals (D), protected individuals who decided to stay at home (P), and protected individuals released who break control measures (P_R). According to the compartmental diagram, as shown in Figure 4.1, the mathematical model is given by

$$
\begin{aligned}
\dot{S} &= -\left(\frac{\alpha_a I_A + \alpha_s I_S}{N^*}\right) S - \omega_1(t) S \\
\dot{P} &= \omega_1(t) S - \left(\frac{\tilde{\alpha}_a I_A + \tilde{\alpha}_s I_S}{N^*}\right) P - \omega_2(t) P \\
\dot{P}_R &= \omega_2(t) P - \left(\frac{\hat{\alpha}_a I_A + \hat{\alpha}_s I_S}{N^*}\right) P_R \\
\dot{E} &= \left(\frac{\alpha_a I_A + \alpha_s I_S}{N^*}\right) S + \left(\frac{\tilde{\alpha}_a I_A + \tilde{\alpha}_s I_S}{N^*}\right) P + \left(\frac{\hat{\alpha}_a I_A + \hat{\alpha}_s I_S}{N^*}\right) P_R - \delta E \\
\dot{I}_A &= (1-\theta)\,\delta E - \eta_a I_A \\
\dot{I}_S &= \theta \delta E - \gamma_s I_S \\
\dot{H} &= \beta \gamma_s I_S + \tau \psi Q - \mu H \\
\dot{Q} &= (1-\beta)\,\gamma_s I_S - \psi Q \\
\dot{R} &= \eta_a I_A + (1-\nu)\,\mu H + (1-\tau)\,\psi Q \\
\dot{D} &= \nu \mu H
\end{aligned}
\tag{4.1}
$$

where $N^* = S + E + I_A + I_S + R + P + P_R$, and

$$\omega_1(t) = \begin{cases} 0 & , \quad 0 \leq t < T_{L_1}, \\ w_{10} & , \quad T_{L_1} \leq t < T_{U_1}, \\ 0 & , \quad T_{U_1} \leq t \ , \end{cases} \tag{4.2}$$

$$\omega_2(t) = \begin{cases} 0 & , \quad 0 \leq t < T_{L_2}, \\ w_{20} & , \quad T_{L_2} \leq t < T_{U_2}, \\ 0 & , \quad T_{U_2} \leq t \ . \end{cases} \tag{4.3}$$

$[T_{L_1}, T_{U_1}]$ represents the period in which the susceptible population move to the protected class until a certain percentage of the population is reached, and $[T_{L_2}, T_{U_2}]$ represents the period in which a percentage of the population that breaks the confinement is reached. Values for ω_{10} is obtained using the following equation:

$$\omega_{10} = \frac{1}{T_{U_1} - T_{L_1}} \ln\left(\frac{1}{k}\right) \tag{4.4}$$

where $(1 - k)$ is the population proportion that is protected until time. Similarly, values for ω_{20} are obtained. Parameter definitions are given in Table (4.1). For details on the model description, see [39].

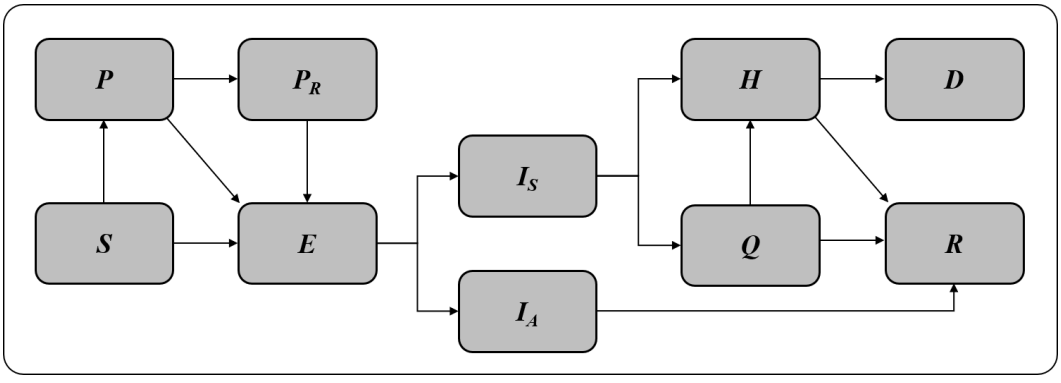

Figure 4.1: Compartmental diagram for the mathematical model. Reprinted from [39].

Parameter	Definition
$\alpha_a, (\tilde{\alpha}_a, \hat{\alpha}_a)$	Transmission contact rates for susceptible (protected, protected released) class linked to asymptomatic individuals
$\alpha_s, (\tilde{\alpha}_s, \hat{\alpha}_s)$	Transmission contact rates for susceptible (protected, protected released) class linked to symptomatic individuals
δ	Incubation rate
θ	Proportion of symptomatic individuals
η_a	Recovery rate for asymptomatic individuals
γ_s	Output rate from the symptomatic class by register
β	Proportion of hospitalized individuals
ψ	Output rate from the quarantined class by hospitalization/recovery
μ	Output rate from the hospitalized class by recovery/death

Table 4.1: Parameter definitions of model (4.1). Reprinted from [39]

4.1.2 Method

The Monte Carlo method considered consists of the following steps.

1. **Initial conditions for the model:** The first COVID-19 case confirmed by the Sonoran Health System was in March 16, 2020, being March 11 the onset symptoms date [84]. Based on this, we consider March 11 as the beginning of the COVID-19 dynamics in Hermosillo for model (4.1) with the initial conditions: $S(0) = 930668$, $I_S(0) = 1$, and $E(0) = I_A(0) = H(0) = D(0) = Q(0) = R(0) = P(0) = P_L(0) = 0$. Total population of Hermosillo for the year 2020 was taken according to the Mexican National Population Council (CONAPO) projections [85].

2. **On-and-off periods of social distancing:** We assumed that the period from March 16 to April 15 was the first period of social distancing, where a considerable proportion of the susceptible population became protected. A second period was fixed from April 30 to May 15. Therefore, we set $[T_{L_1}, T_{U_1}]$ and $[T_{L_2}, T_{U_2}]$ as $[5, 35]$ and $[50, 65]$, respectively.

3. **Model parameter distributions:** We selected a set of distributions for model parameters given in Table 4.2. The selection of the probability distributions was based both on previous experience and the versatility of certain distributions. An initial fit of the model solutions was made to the data reported through an application created in RStudio [86]. The latter allowed to delimit the supports of these distributions considering wide ranges and a bibliographic review given in Table 4.3 as a starting point.

Parameter	Distribution	Parameter	Distribution
α_a	$\mathcal{N}_{0,\infty}(1.198, 0.05)$	γ_s	$\mathcal{IG}(3, 1)$
α_s	$\mathcal{N}_{0,\infty}(0.657, 0.05)$	β	$\mathcal{B}(8, 50)$
$\tilde{\alpha}_a$	$\mathcal{N}_{0,\infty}(0.02, 0.05)$	τ	$\mathcal{U}(0.1, 0.3)$
$\tilde{\alpha}_s$	$\mathcal{N}_{0,\infty}(0.02, 0.05)$	ψ	$\mathcal{U}(0.06, 0.1)$
$\hat{\alpha}_a$	$\mathcal{N}_{0,\infty}(0.02, 0.05)$	μ	$\mathcal{U}(0.05, 0.1)$
$\hat{\alpha}_s$	$\mathcal{N}_{0,\infty}(0.02, 0.05)$	ν	$\mathcal{U}(0.2, 0.4)$
δ	$\mathcal{IG}(25, 5)$	w_{10}	$\mathcal{U}(0.04, 0.08)$
θ	$\mathcal{U}(0.17, 0.25)$	w_{20}	$\mathcal{U}(0.007, 0.03)$
η_a	$\mathcal{IG}(105, 10)$	-	-

Table 4.2: Model parameter distributions.

In particular, distributions for ω_{10} and ω_{20} were obtained assuming a $\mathcal{U}(0.7, 0.9)$ distribution for the protected proportion of susceptible individuals and a $\mathcal{U}(0.1, 0.35)$ distribution for the proportion of people who have broken the confinement. Once we have a sample for each proportion, we applied the equation (4.4) to these samples, considering that protected and released population proportions are achieved within 30 and 15 days, respectively. The values obtained for ω_{10} and ω_{20} allowed us to propose the corresponding distributions given in Table 4.2 and the parameters range shown in Table 4.3.

Parameter	Reference	Parameter	Reference
α_a	0.5944–1.68 [87]	$1/\gamma_s$	0.8–8.2 [88]
α_s	0.5944–1.68 [87]	β	0.1–0.3*
$\tilde{\alpha}_a$	0–0.5*	τ	0–0.5*
$\tilde{\alpha}_s$	0–0.5*	$1/\psi$	8.2–15.6 [89]
$\hat{\alpha}_a$	0–0.5*	$1/\mu$	4.7–10.3*; 11-25 [90]
$\hat{\alpha}_s$	0–0.5*	ν	0–0.4*
$1/\delta$	2–14 [91]	w_{10}	0.04–0.08*
θ	0–0.8*	w_{20}	0.007–0.03*
$1/\eta_a$	8.2–15.6 [89]	-	-

Table 4.3: Initial parameter ranges and values, taken from current literature or assumed (*).

4. **Empirical constraint on prevalence:** Based on a prevalence study carried out in Spain [92], we include solutions where the cumulative number of infected people, from the first case until day 200, were at most 21.6% of the total population in Hermosillo.

5. **Data.** The dataset used was downloaded from the official website of the Mexican Federal Government on July 19, 2020 [84]. According to some lifting confinement measures adopted by the Mexican government, the study period was from March 11 to May 31. The cases considered for the study were the positive cases for SARS-CoV-2 with residence in Hermosillo and treated in a medical unit in the Sonora state. The selected variables were daily cases by symptom onset date, hospitalized and ambulatory by date of admission to a health service unit, and daily deaths (see Figure 4.2).

6. **Empirical restriction on epidemic curves:** To ensure reasonable solutions, we considered an inclusion criterion that consisted of selecting those solutions whose sum of squared errors about the data was smaller than some specific upper bound. For this, we perform the following steps:

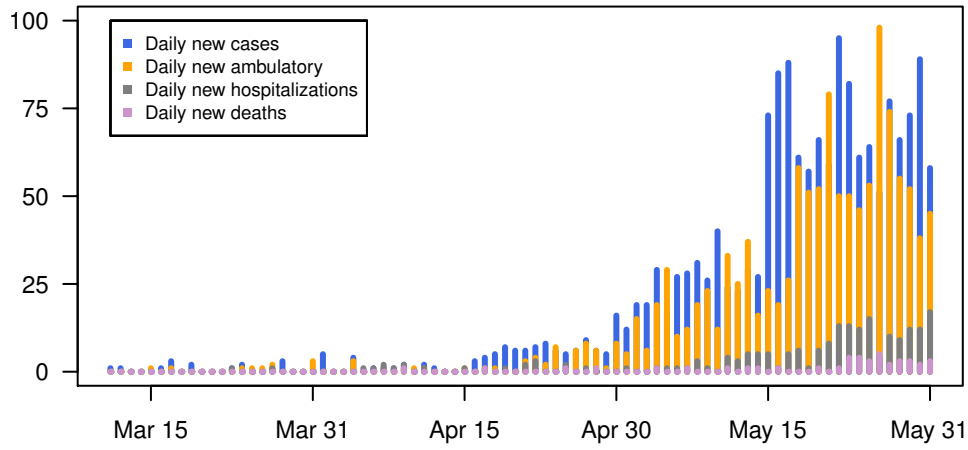

Figure 4.2: COVID-19 data from Hermosillo from March 11 to May 31 [84].

Step 1 We first define the following variables with respect model (4.1):

$$\begin{aligned} DI_S(k) &= \int_{k-1}^{k} \theta\delta E(t)\,dt, \\ DH(k) &= \int_{k-1}^{k} \beta\gamma_s I_s(t)\,dt, \\ DQ(k) &= \int_{k-1}^{k} (1-\beta)\gamma_s I_s(t)\,dt, \\ DD(k) &= \int_{k-1}^{k} \nu\mu H(t)\,dt. \end{aligned} \tag{4.5}$$

where $DI_S(k)$, $DH(k)$, $DQ(k)$, and $DD(k)$ are the number of symptomatic infected, hospitalized, ambulatory and death cases, respectively, on the kth day.

Step 2 Then, we obtained $m = 1000$ parameter samples set according to the distributions defined for model parameters in Table 4.2 and, for each parameter sample set, we solve system (4.1) and calculate the sums of

squared errors given by

$$\begin{aligned} SSE(I_S) &= \sum_{k=1}^{82} (x_k - DI_S(k))^2 , \\ SSE(H) &= \sum_{k=1}^{82} (y_k - DH(k))^2 , \\ SSE(Q) &= \sum_{k=1}^{82} (z_k - DQ(k))^2 , \\ SSE(D) &= \sum_{k=1}^{82} (w_k - DD(k))^2 , \end{aligned} \tag{4.6}$$

where x_k, y_k, z_k, and w_k represent the daily data of symptomatic infected, hospitalized, ambulatory, and deaths, respectively, at day k, shown in Figure 4.2.

Step 3 Finally, once the 1000 sets of sums of squared errors are obtained, we calculate the 25th percentile of the sum of the squared errors for each variable. It is considered the upper bound to admit solutions for system (4.1).

4.2 Results

We obtained 5000 solutions from system (4.1) that hold the criteria previously explained. Figure 4.3 shows the band that covers the 5000 solution curves obtained for daily new cases by symptom onset date (DIs), daily hospitalized (DH) and ambulatory (DQ) by date of admission to a medical unit, and deaths daily (DD). We can observe a good fit of the real data to the solution curves obtained. In Figure 4.4, we can see the histograms of the parameter values obtained after applying the proposed methodology.

According to the solution curves obtained for Figure 4.3, we calculate the date

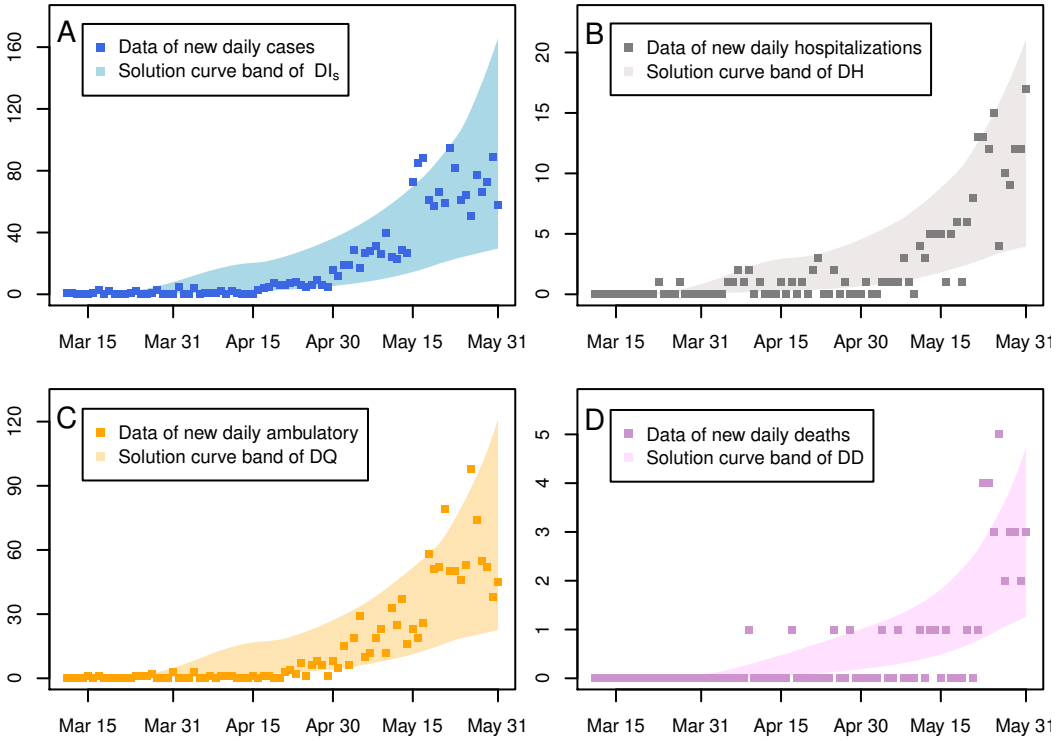

Figure 4.3: Solution curve bands for new daily cases (A), new daily hospitalizations (B), new daily ambulatory (C), and new daily deaths (D).

of occurrence of the acme for every one of the solutions. Figure 4.5 shows the distributions of the estimated date of the acme for the daily new reported, hospitalized, ambulatory, and death variables. The 95% quantile-based interval is from July 13 to August 30 for the peak of cases, from July 16 to September 2 for the peak of hospitalizations, from August 3 to September 22 for the peak of deaths. In particular, the median date for the acme of incidence cases occurs on August 3, which is a date close to the peak of incidence that happened in Hermosillo (around the 31st epidemiological week).

Finally, we evaluate implications on the prevalence of hospitalized and the cumulative deaths if the lockdown had been implemented one or two weeks later than our real scenario. For this, we calculate the quantile 0.5 for each parameter

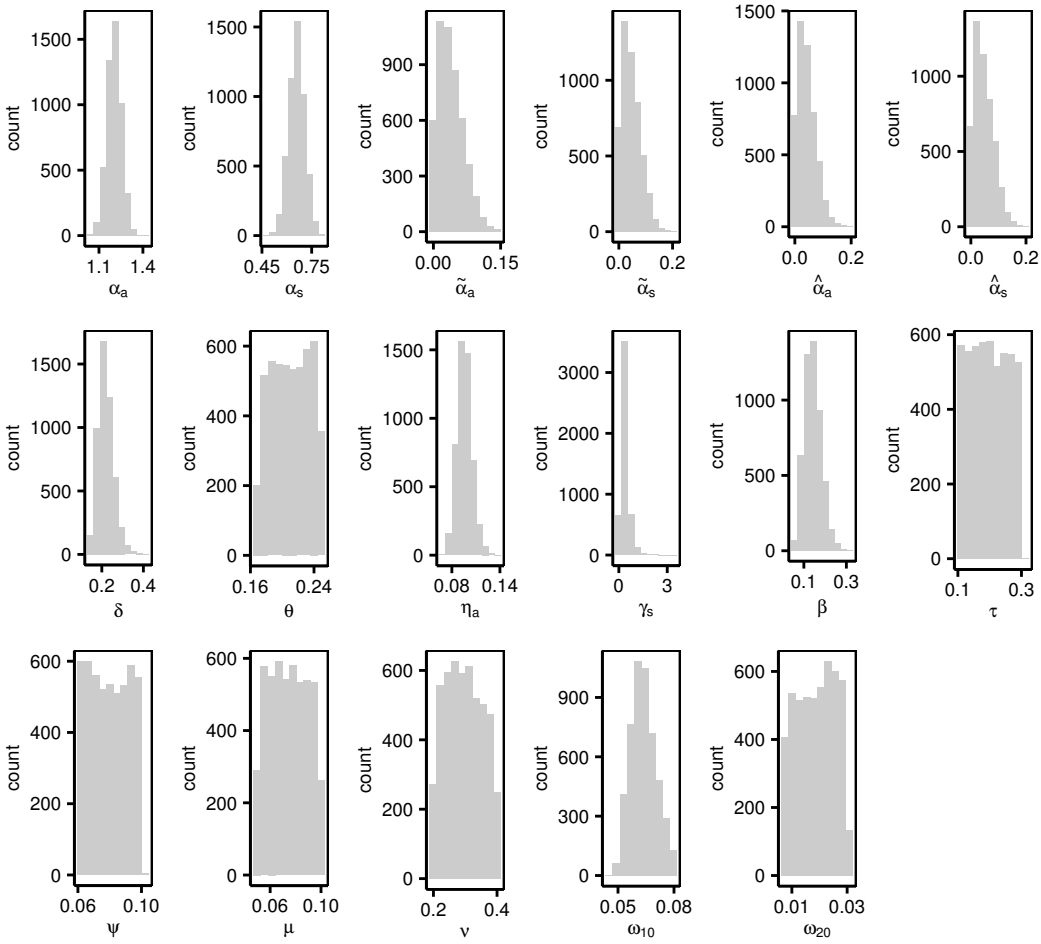

Figure 4.4: Histogram for each one of the parameters.

of all 5000 combinations, and, with these values, we obtain our baseline scenario (lockdown from March 16 to April 15). We carried out simulations considering that lockdown took place over a time interval from March 23 to April 22 and from March 30 to April 29. Figure 4.6 shows the solution for our baseline scenario and those two hypothetical scenarios. We observe that a significant increase in the number of daily new hospitalizations and cumulative deaths would have occurred if lockdown had taken one or two weeks after the original date.

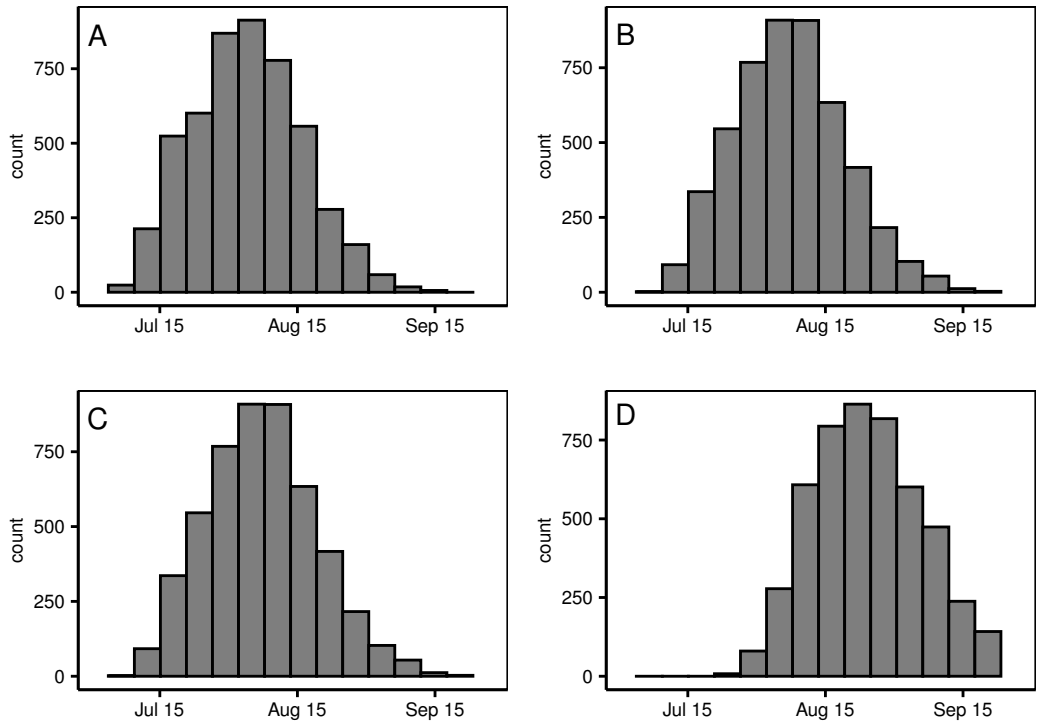

Figure 4.5: Histograms of acme dates for the epidemic curves: daily new reported cases (A), daily hospitalizations (B), daily ambulatory (C), and daily deaths (D).

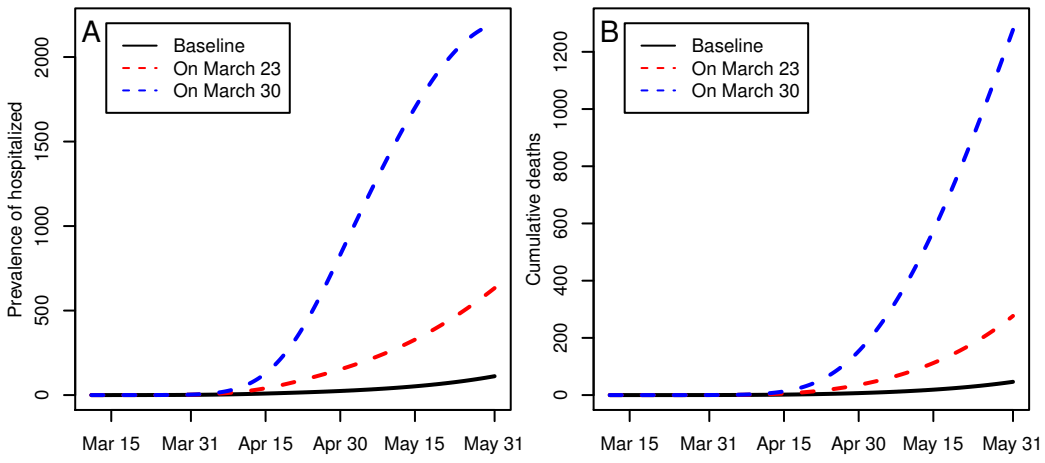

Figure 4.6: Implications of the delay of one or two weeks regarding the time of occurrence of lockdown. Prevalence of hospitalized (A) and cumulative deaths (B).

4.3 Conclusions and discussions

Since the characteristics of COVID-19 are not well known yet, it was more appropriate to consider different scenarios for model parameters. Thus, a Monte Carlo study was more suited to fit the data. In [39], we can see the other two sets of selected distributions also provide solutions that fit the data. This fact highlights the parameter identifiability problem.

Based on the proposed scenario, the model described the temporal dynamic of the COVID-19 in Hermosillo. Moreover, the acme occurrence time is close to the real date of Hermosillo. Although the other two sets of distributions proposed by two other researchers do not totally coincide with the one presented here, the dynamics preserved the property of the acme occurrence time.

We also explore the hypothetical delay of one and two weeks of the implementation of lockdown measures. According to our scenario, a week late would have led to about five times more accumulated deaths than what was obtained in our dynamic baseline, by May 31, whereas a two-week late would have increased about 26 times. Thus, the measures applied on March 16 allowed to avoid a high number of deaths and hospitalizations.

Chapter 5

General conclusions

In this work, we have proposed theoretical-numerical and applied approaches to explore scenarios in infectious disease dynamics. Although the approaches were applied to Dengue and COVID-19, they can be adapted according to problems that need to be addressed and applied to infectious diseases such as Chikungunya, Zika, or SARS, among others. Moreover, information about applied control strategies (dates and locations), mobility patterns of humans and vectors, or reliable data of cases may generate more realistic scenarios, which may be helpful for decision-making in public health.

The use of GIS, socio-demographic and socio-economic information played an important role throughout this work because they allowed us to delimit appropriate study areas. These tools helped us to identify heterogeneous conditions for the disease spread in the city of Hermosillo. Moreover, we recognized behaviors in the dengue data associated with spatio-temporal dynamics; for example, the double peak of cases observed in Figure 1.1 of Chapter 1. Therefore, we believe these tools are essential to comprehend the spatio-temporal dynamics better and formulate more appropriate hypotheses of mathematical models.

Chapters 2 and 3 allowed us to emphasize the role of human mobility in the spread of infectious diseases. Although it was not possible to find the expression of the global R_0 for the model, the local basic reproductive numbers were used as indicators

of favorable conditions for the existence or not of endemic equilibria and outbreaks. Identifying the local conditions for the spread of infectious diseases in a population can allow to focus control measures better and avoid spreading to another neighborhood. Future works may use the modeling approach to a network of connected patches to study the infectious disease dynamics, where the patches may be defined considering socio-economic and socio-demographic information, and mobility patterns.

In Chapters 1 and 3, we have used statistical methods to obtain reasonable values of the parameters and propose hypothetical scenarios. First, we identified the parameter values that needed to be fixed at specific values. Then, we employed the Bayesian approach to obtain different scenarios due to the lack of available information. Here, Bayesian approach was used in another way what is traditionally applied. On the other hand, due to some characteristics of the COVID-19 disease are not very clear yet, we needed another way to explore scenarios. For example, the role of asymptomatic individuals in the disease dynamics is not entirely clear yet. In this context, together with other researchers, we presented a methodology based on the Monte Carlo method to obtain different scenarios by proposing different sets of distributions for the model parameters. As we have seen in Chapter 4, we believe that sometimes we must evaluate other alternatives before estimating parameters because there could be a parameter identifiability problem serious.

Bibliography

[1] Mayo Clinic. Infectious diseases. https://www.mayoclinic.org/diseases-conditions/infectious-diseases/symptoms-causes/syc-20351173?p=1. Accessed January 26, 2021.

[2] Uzma Khan, Roopa Mehta, Mohammad A. Arif, and Om J. Lakhani. Pandemics of the past: A narrative review. *The Journal of the Pakistan Medical Association*, 70(5):S34–S37, 2020. doi:10.5455/JPMA.11.

[3] WHO. World malaria report 2020: 20 years of global progress and challenges. November 2020. https://www.who.int/publications/i/item/9789240015791. Accessed January 26, 2021.

[4] WHO. Dengue and severe dengue. June 2020. https://www.who.int/news-room/fact-sheets/detail/dengue-and-severe-dengue. Accessed December 15, 2019.

[5] PAHO. Plataforma de Información en Salud para las Américas (PLISA). https://www.paho.org/data/index.php/es/temas/indicadores-dengue/dengue-nacional/9-dengue-pais-ano.html?start=2. Accessed December 1, 2020.

[6] Ensheng Dong, Hongru Du, and Lauren Gardner. COVID-19 in real time. *The Lancet Infectious Diseases*, 20(5):533–534, 2020. doi:10.1016/S1473-3099(20)30120-1.

[7] Peter N. Fonkwo. Pricing infectious disease. the economic and health

implications of infectious diseases. *EMBO Reports*, 9:S13–S17, 2008. doi:10.1038/embor.2008.110.

[8] Eduardo A. Undurraga, Miguel Betancourt-Cravioto, José Ramos-Castañeda, Ruth Martínez-Vega, Jorge Méndez-Galván, Duane J. Gubler, María G. Guzmán, Scott B. Halstead, Eva Harris, Pablo Kuri-Morales, Roberto Tapia-Conyer, and Donald S. Shepard. Economic and Disease Burden of Dengue in Mexico. *PLoS Neglected Tropical Diseases*, 9(3):1–26, 2015. doi:10.1371/journal.pntd.0003547.

[9] T. Ibn-Mohammed, K.B. Mustapha, J. Godsell, Z. Adamu, K.A. Babatunde, D.D. Akintade, A. Acquaye, H. Fujii, M.M. Ndiaye, F.A. Yamoah, and S.C.L. Koh. A critical analysis of the impacts of covid-19 on the global economy and ecosystems and opportunities for circular economy strategies. *Resources, Conservation & Recycling*, 164:105169, 2021. doi:10.1016/j.resconrec.2020.105169.

[10] Rima F. Khabbaz, Robin R. Moseley, Riley J. Steiner, Alexandra M. Levitt, and Beth P. Bell. Challenges of infectious diseases in the USA. *The Lancet*, 384 (9937):53–63, 2014. doi:10.1016/S0140-6736(14)60890-4.

[11] Vittoria Colizza, Alain Barrat, Marc Barthélemy, and Alessandro Vespignani. The role of the airline transportation network in the prediction and predictability of global epidemics. *Proceedings of the National Academy of Sciences*, 103(7): 2015–2020, 2006. doi:10.1073/pnas.0510525103.

[12] Aidan Findlater and Isaac I Bogoch. Human Mobility and the Global Spread of Infectious Diseases: A Focus on Air Travel. *Trends in Parasitology*, 34(9): 772–783, 2018. doi:10.1016/j.pt.2018.07.004.

[13] Ben Adams and Durrell D. Kapan. Man bites mosquito: Understanding the

contribution of human movement to vector-borne disease dynamics. *PLoS ONE*, 4(8):e6763, 2009. doi:10.1371/journal.pone.0006763.

[14] Suttikiat Changruenngam, Dominique J Bicout, and Charin Modchang. How the individual human mobility spatio - temporally shapes the disease transmission dynamics. *Scientific Reports*, pages 1–13, 2020. doi:10.1038/s41598-020-68230-9.

[15] Sameer Saran, Priyanka Singh, Vishal Kumar, and Prakash Chauhan. Review of Geospatial Technology for Infectious Disease Surveillance: Use Case on COVID-19. *Journal of the Indian Society of Remote Sensing*, 48(8):1121–1138, 2020. doi:10.1007/s12524-020-01140-5.

[16] Fred Brauer and Carlos Castillo-Chavez. *Mathematical Models in Population Biology and Epidemiology*. Texts in Applied Mathematics. Second edition, 2012. ISBN 9781461416869.

[17] Abhishek Pandey, Anuj Mubayi, and Jan Medlock. Comparing vector – host and sir models for dengue transmission. *Mathematical Biosciences*, 246(2):252–259, 2013. doi:10.1016/j.mbs.2013.10.007.

[18] Adnan Khan, Muhammad Hassan, and Mudassar Imran. Estimating the basic reproduction number for single-strain dengue fever epidemics. *Infectious Diseases of Poverty*, 3:12, 2014. doi:10.1186/2049-9957-3-12.

[19] Dao N. Vinh, Dang Thi, Minh Ha, Nguyen T. Hanh, Guy Thwaites, Maciej F. Boni, Hannah E. Clapham, Nguyen Thuy, and Thuong Thuong. Modeling tuberculosis dynamics with the presence of hyper-susceptible individuals for Ho Chi Minh City from 1996 to 2015. *BMC Infectious Diseases*, 18:494, 2018. doi:10.1186/s12879-018-3383-3.

[20] Necibe Tuncer, Chindu Mohanakumar, Samuel Swanson, and Maia Martcheva. Efficacy of control measures in the control of Ebola, Liberia

2014 – 2015. *Journal of Biological Dynamics*, 12(1):913–937, 2018. doi:10.1080/17513758.2018.1535095.

[21] Sourav Kumar, Sasmal Indrajit, and Ghosh Amit. Modeling the Spread of Zika Virus in a Stage-Structured Population: Effect of Sexual Transmission. *Bulletin of Mathematical Biology*, 80(11):3038–3067, 2018. doi:10.1007/s11538-018-0510-7.

[22] Indrajit Ghosh, Pankaj Kumar, Sudip Samanta, Ibrahim M Elmojtaba, and Nasser Al-salti. A simple SI-type model for HIV/AIDS with media and self-imposed psychological fear. *Mathematical Biosciences*, 306:160–169, 2018. doi:10.1016/j.mbs.2018.09.014.

[23] Longxing Qi, Meng Xue, Jing-an C. Qizhi, and Wang Tianping. Schistosomiasis Transmission Model and its Control in Anhui Province. *Bulletin of Mathematical Biology*, 80(9):2435–2451, 2018. doi:10.1007/s11538-018-0474-7.

[24] Van K. Nguyen, César Parra-rojas, and Esteban A. Hernandez-vargas. The 2017 plague outbreak in Madagascar: Data descriptions and epidemic modelling. *Epidemics*, 25:20–25, 2019. doi:10.1016/j.epidem.2018.05.001.

[25] Chris Cosner. Models for the effects of host movement in vector-borne disease systems. *Mathematical Biosciences*, 270:192–197, 2015. doi:10.1016/j.mbs.2015.06.015.

[26] M. A. Aziz-Alaoui, Sunita Gakkhar, Benjamin Ambrosio, and Arti Mishra. A network model for control of dengue epidemic using sterile insect technique. *Mathematical Biosciences and Engineering*, 15(2):441–460, 2017. doi:10.3934/mbe.2018020.

[27] Arti Mishra and Sunita Gakkhar. Non-linear Dynamics of Two-Patch Model

Incorporating Secondary Dengue Infection. *International Journal of Applied and Computational Mathematics*, 4:19, 2018. doi:10.1007/s40819-017-0460-z.

[28] Ross William S. Hendron and Michael B. Bonsall. The interplay of vaccination and vector control on small dengue networks. *Journal of Theoretical Biology*, 407:349–361, 2016. doi:10.1016/j.jtbi.2016.07.034.

[29] Yanyu Xiao and Xingfu Zou. Transmission dynamics for vector-borne diseases in a patchy environment. *Journal of Mathematical Biology*, 69(1):113–146, 2014. doi:10.1007/s00285-013-0695-1.

[30] Julien Arino and P. Van Den Driessche. A multi-city epidemic model. *Mathematical Population Studies*, 10(3):175–193, 2003. doi:10.1080/08898480306720.

[31] Ganga Ram Phaijoo and Dil Bahadur Gurung. Mathematical Study of Dengue Disease Transmission in Multi-Patch Environment. *Applied Mathematics*, 7(14): 1521–1533, 2016. doi:10.4236/am.2016.714132.

[32] Sunmi Lee and Carlos Castillo-Chavez. The role of residence times in two-patch dengue transmission dynamics and optimal strategies. *Journal of Theoretical Biology*, 374:152–164, 2015. doi:10.1016/j.jtbi.2015.03.005.

[33] Derdei Bichara and Carlos Castillo-Chavez. Vector-borne diseases models with residence times - A Lagrangian perspective. *Mathematical Biosciences*, 281: 128–138, 2016. doi:10.1016/j.mbs.2016.09.006.

[34] Jung E. Kim, Hyojung Lee, Chang H. Lee, and Sunmi Lee. Assessment of optimal strategies in a two-patch dengue transmission model with seasonality. *PLoS ONE*, 12(3):e0173673, 2017. doi:10.1371/journal.pone.0173673.

[35] Edwin Barrios, Sunmi Lee, and Olga Vasilieva. Assessing the effects of daily

commuting in two-patch dengue dynamics: A case study of Cali, Colombia. *Journal of Theoretical Biology*, 453:14–39, 2018. doi:10.1016/j.jtbi.2018.05.015.

[36] Emmanuel A. Mpolya, Kenta Yashima, Hisashi Ohtsuki, and Akira Sasaki. Epidemic dynamics of a vector-borne disease on a villages-and-city star network with commuters. *Journal of Theoretical Biology*, 343:120–126, 2014. doi:10.1016/j.jtbi.2013.11.024.

[37] Kimberlyn Roosa and Gerardo Chowell. Assessing parameter identifiability in compartmental dynamic models using a computational approach: application to infectious disease transmission models. *Theoretical Biology and Medical Modelling*, 16:1, 2019. doi:10.1186/s12976-018-0097-6.

[38] Gudelia Figueroa Preciado, José A. Montoya Laos, Daniel Olmos Liceaga, Manuel A. Acuña Zegarra, Jesús A. Minjárez Sosa, Benjamín Burgos Flores, and Pablo A and Reyes Castro. Reporte Preliminar del Equipo de Biomatemática. Escenarios de Modelación. https://www.unison.mx/wp-content/uploads/2020/05/Reporte-Biomatematica-entregado-a-la-Secretaria-de-Salud-mayo7-2020.pdf. Accessed December 1, 2020.

[39] Mayra R. Tocto-Erazo, Jorge A. Espíndola-Zepeda, José A. Montoya-Laos, Manuel A. Acuña-Zegarra, Daniel Olmos-liceaga, Pablo A. Reyes-castro, and Gudelia Figueroa-Preciado. Lockdown, relaxation, and acme period in COVID-19: A study of disease dynamics in Hermosillo, Sonora, Mexico. *PLoS ONE*, 15(12):e0242957, 2020. doi:10.1371/journal.pone.0242957.

[40] Mayra R. Tocto-Erazo, Daniel Olmos-Liceaga, and José A. Montoya-Laos. Effect of daily human movement on some characteristics of dengue dynamics. *Mathematical Biosciences*, 332:108531, 2020. doi:10.1016/j.mbs.2020.108531.

[41] Mayra R. Tocto-Erazo, Daniel Olmos-Liceaga, and José A. Montoya-Laos. Effect of daily periodic human movement on dengue dynamics: The case of the 2010

outbreak in hermosillo, mexico. *Applied Mathematical Modelling*, 97:559–567, 2021. doi:10.1016/j.apm.2021.04.001.

[42] S. Bhatt, P.W. Gething, O.J. Brady, J.P. Messina, A.W. Farlow, C.L. Moyes, J.M. Drake, J.S Brownstein, A.G. Hoen, O. Sankoh, M.F. Myers, D.B. George, T. Jaenisch, G.R. Wint, C.P. Simmons, T.W. Scott, J.J. Farrar, and S.I. Hay. The global distribution and burden of dengue. *Nature*, 496:504–507, 2013. doi:10.1038/nature12060.

[43] Julia Harrington, Axel Kroeger, Silvia Runge-Ranzinger, and Tim O'Dempsey. Detecting and responding to a dengue outbreak: Evaluation of existing strategies in country outbreak response planning. *Journal of Tropical Medicine*, 2013: 756832, 2013. doi:10.1155/2013/756832.

[44] Qinlong Jing and Ming Wang. Dengue epidemiology. *Global Health Journal*, 3 (2):37–45, 2019. doi:10.1016/j.glohj.2019.06.002.

[45] WHO. Global strategy for dengue prevention and control, 2012-2020. 2012. https://apps.who.int/iris/bitstream/handle/10665/75303/9789241504034_eng.pdf. Accessed December 1, 2018.

[46] Kacey C. Ernst, Kathleen R. Walker, Pablo Reyes-Castro, Teresa K. Joy, A. Lucia Castro-Luque, Rolando E. Diaz-Caravantes, Mercedes Gameros, Steven Haenchen, Mary H. Hayden, Andrew Monaghan, Eileen Jeffrey-Guttierez, Yves Carrière, and Michael R. Riehle. Aedes aegypti (Diptera: Culicidae) Longevity and Differential Emergence of Dengue Fever in Two Cities in Sonora, Mexico. *Journal of Medical Entomology*, 54(1):204–211, 2016. doi:10.1093/jme/tjw141.

[47] Secretaría de Salud. Manual de procedimientos estandarizados para la vigilancia epidemiológica de las enfermedades transmitidas por vectores. https://salud.edomex.gob.mx/cevece/documentos/acerca_de/marco_j/manualesvep/Manual_ETV.pdf. Accessed March 5, 2021.

[48] K. Carbajal. Suben los casos de dengue a 215. *El Imparcial*, October 2010. https://www.elimparcial.com/EdicionDigital/.

[49] M. Acuña. Suben a 1000% casos de dengue en la ciudad. *El Imparcial*, October 2010. https://www.elimparcial.com/EdicionDigital/.

[50] Gobierno Municipal de Hermosillo. Boletin informativo 557: Acciones contra el dengue y la rickettsia. July 2010. https://www.hermosillo.gob.mx/boletines/?articleid=2087. Accessed June 20, 2019.

[51] Gobierno Municipal de Hermosillo. Boletin informativo 607: Libran hogares de cacharros. August 2010. https://www.hermosillo.gob.mx/boletines/?articleid=2144. Accessed June 20, 2019.

[52] Gobierno Municipal de Hermosillo. Boletin informativo 702: Descacharre en la ciudad, 2010. November 2010. https://www.hermosillo.gob.mx/boletines/?articleid=2300. Accessed June 20, 2019.

[53] Gobierno Municipal de Hermosillo. Boletin informativo 747: Sigue la limpieza de patios y frentes de casas, 2010. December 2010. https://www.hermosillo.gob.mx/boletines/?articleid=2353. Accessed June 20, 2019.

[54] Pablo A. Reyes-Castro, Robin B. Harris, Heidi E. Brown, Gary L. Christopherson, and Kacey C. Ernst. Spatio-temporal and neighborhood characteristics of two dengue outbreaks in two arid cities of Mexico. *Acta Tropica*, 167:174–182, 2017. doi:10.1016/j.actatropica.2017.01.001.

[55] Consejo Nacional de Población. Índice de marginación (carencias poblacionales) por localidad, municipio y entidad. https://datos.gob.mx/busca/dataset/indice-de-marginacion-carencias-poblacionales-por-localidad-municipio-y-entidad. Accessed June 20, 2019.

[56] Lourdes Esteva and Cristobal Vargas. Analysis of a dengue disease transmission model. *Mathematical Biosciences*, 150(2):131–151, 1998. doi:10.1016/S0025-5564(98)10003-2.

[57] Quirine A. ten Bosch, Hannah E. Clapham, Louis Lambrechts, Veasna Duong, Philippe Buchy, Benjamin M. Althouse, Alun L. Lloyd, Lance A. Waller, Amy C. Morrison, Uriel Kitron, Gonzalo M. Vazquez-Prokopec, Thomas W. Scott, and T. Alex Perkins. Contributions from the silent majority dominate dengue virus transmission. *PLoS Pathogens*, 14(5):82–86, 2018. doi:10.1371/journal.ppat.1006965.

[58] G. Chowell, P. Diaz-Dueñas, J. C. Miller, A. Alcazar-Velazco, J. M. Hyman, P. W. Fenimore, and C. Castillo-Chavez. Estimation of the reproduction number of dengue fever from spatial epidemic data. *Mathematical Biosciences*, 208(2): 571–589, 2007. doi:10.1016/j.mbs.2006.11.011.

[59] Mathieu Andraud, Niel Hens, Christiaan Marais, and Philippe Beutels. Dynamic epidemiological models for dengue transmission: a systematic review of structural approaches. *PloS ONE*, 7(11):e49085, 2012. doi:10.1371/journal.pone.0049085.

[60] Siddhartha Chib and Edward Greenberg. Understanding the metropolis-hastings algorithm. *The American Statistician*, 49(4):327–335, 1995. doi:10.1080/00031305.1995.10476177.

[61] M. N. Burattini, M. Chen, A. Chow, F. A. B. Coutinho, K. T. Goh, L. F. Lopez, S. MA, and E. Massad. Modelling the control strategies against dengue in Singapore. *Epidemiology and Infection*, 136(3):309–319, 2008. doi:10.1017/S0950268807008667.

[62] Gerhart Knerer, Christine S.M. Currie, and Sally C. Brailsford. Impact of combined vector-control and vaccination strategies on transmission dynamics

of dengue fever: a model-based analysis. *Health Care Management Science*, 18 (2):205–217, 2015. doi:10.1007/s10729-013-9263-x.

[63] Meksianis Z. Ndii, David Allingham, R. I. Hickson, and Kathryn Glass. The effect of Wolbachia on dengue outbreaks when dengue is repeatedly introduced. *Theoretical Population Biology*, 111:9–15, 2016. doi:10.1016/j.tpb.2016.05.003.

[64] Joseph Páez Chávez, Thomas Götz, Stefan Siegmund, and Karunia Putra Wijaya. An SIR-Dengue transmission model with seasonal effects and impulsive control. *Mathematical Biosciences*, 289:29–39, 2017. doi:10.1016/j.mbs.2017.04.005.

[65] Arti Mishra, Benjamin Ambrosio, Sunita Gakkhar, and M. A. Aziz-Alaoui. A network model for control of dengue epidemic using sterile insect technique. *Mathematical Biosciences and Engineering*, 15(2):441–460, 2018. doi:10.3934/mbe.2018020.

[66] Abhishek Senapati, Tridip Sardar, Krishnendra S. Ganguly, Krishna S. Ganguly, Asis K. Chattopadhyay, and Joydev Chattopadhyay. Impact of adult mosquito control on dengue prevalence in a multi-patch setting: A case study in Kolkata (2014–2015). *Journal of Theoretical Biology*, 478:139–152, 2019. doi:10.1016/j.jtbi.2019.06.021.

[67] Oliver J. Brady, Peter W. Gething, Samir Bhatt, Jane P. Messina, John S. Brownstein, Anne G. Hoen, Catherine L. Moyes, Andrew W. Farlow, Thomas W. Scott, and Simon I. Hay. Refining the Global Spatial Limits of Dengue Virus Transmission by Evidence-Based Consensus. *PLoS Neglected Tropical Diseases*, 6(8), 2012. doi:10.1371/journal.pntd.0001760.

[68] Steven T. Stoddard, Amy C. Morrison, Gonzalo M. Vazquez-Prokopec, Valerie P. Soldan, J. Tadeusz, Uriel Kitron, John P. Elder, and Thomas W. Scott. The Role

of Human Movement in the Transmission of Vector-Borne Pathogens. *PLoS neglected tropical diseases*, 3(7):e481, 2009. doi:10.1371/journal.pntd.0000481.

[69] Steven T. Stoddard, Brett M. Forshey, Amy C. Morrison, Valerie A. Paz-Soldan, Gonzalo M. Vazquez-Prokopec, Helvio Astete, Robert C. Reiner, Stalin Vilcarromero, John P. Elder, Eric S. Halsey, Tadeusz J. Kochel, Uriel Kitron, and Thomas W. Scott. House-to-house human movement drives dengue virus transmission. *Proceedings of the National Academy of Sciences of the United States of America*, 110(3):994–999, 2013. doi:10.1073/pnas.1213349110.

[70] Hamish P. Mohammed, Mary M. Ramos, Aidsa Rivera, Michael Johansson, Jorge L. Muñoz-Jordan, Wellington Sun, and Kay M. Tomashek. Travel-associated dengue infections in the United States, 1996 to 2005. *Journal of Travel Medicine*, 17(1):8–14, 2010. doi:10.1111/j.1708-8305.2009.00374.x.

[71] Kevin R Porter, Charmagne G Beckett, Herman Kosasih, Ratna Irsiana Tan, Bachti Alisjahbana, Pandji Irani, Fianza Rudiman, Susana Widjaja, and Erlin Listiyaningsih. Epidemiology of dengue and dengue hemorrhagic fever in a cohort of adults living in Bandung, West Java, Indonesia. *The American Journal of Tropical Medicine and Hygiene*, 72(1):60–66, 2005. doi:10.4269/ajtmh.2005.72.60.

[72] Fred Brauer, Carlos Castillo-Chavez, Anuj Mubayi, and Sherry Towers. Some models for epidemics of vector-transmitted diseases. *Infectious Disease Modelling*, 1(1):79–87, 2016. doi:10.1016/j.idm.2016.08.001.

[73] Max O. Souza. Multiscale analysis for a vector-borne epidemic model. *Journal of Mathematical Biology*, 68(5):1269–1293, 2014. doi:10.1007/s00285-013-0666-6.

[74] Manuel A. Acuña-Zegarra, Daniel Olmos-Liceaga, and Jorge X. Velasco-Hernández. The role of animal grazing in the spread of Chagas disease. *Journal of Theoretical Biology*, 457:19–28, 2018. doi:10.1016/j.jtbi.2018.08.025.

[75] Guanghu Zhu, Tao Liu, Jianpeng Xiao, Bing Zhang, Tie Song, Yonghui Zhang, Lifeng Lin, Zhiqiang Peng, Aiping Deng, Wenjun Ma, and Yuantao Hao. Effects of human mobility, temperature and mosquito control on the spatiotemporal transmission of dengue. *Science of the Total Environment*, 651:969–978, 2019. doi:10.1016/j.scitotenv.2018.09.182.

[76] Hugo Barbosa, Marc Barthelemy, Gourab Ghoshal, Charlotte R James, Maxime Lenormand, Thomas Louail, Ronaldo Menezes, José J Ramasco, Filippo Simini, and Marcello Tomasini. Human mobility: Models and applications. *Physics Reports*, 734:1–74, 2018. doi:10.1016/j.physrep.2018.01.001.

[77] G. Chowell and R. Rothenberg. Spatial infectious disease epidemiology: on the cusp. *BMC Medicine*, 16(1):192, 2018. doi:10.1186/s12916-018-1184-6.

[78] A. Anzo-Hernández, B. Bonilla-Capilla, J. Velázquez-Castro, M. Soto-Bajo, and A. Fraguela-Collar. The risk matrix of vector-borne diseases in metapopulation networks and its relation with local and global R0. *Communications in Nonlinear Science and Numerical Simulation*, 68:1–14, 2019. doi:10.1016/j.cnsns.2018.06.006.

[79] Jorge A. Falcón-Lezama, Ruth A. Martínez-Vega, Pablo A. Kuri-Morales, José Ramos-Castañeda, and Ben Adams. Day-to-Day Population Movement and the Management of Dengue Epidemics. *Bulletin of Mathematical Biology*, 78(10): 2011–2033, 2016. doi:10.1007/s11538-016-0209-6.

[80] Emilene Pliego Pliego, Jorge Velázquez-Castro, Markus P. Eichhorn, and Andrés Fraguela Collar. Increased efficiency in the second-hand tire trade provides opportunity for dengue control. *Journal of Theoretical Biology*, 437:126–136, 2018. doi:10.1016/j.jtbi.2017.10.025.

[81] A. Iggidr, J. Koiller, M. L.F. Penna, G. Sallet, M. A. Silva, and M. O. Souza. Vector borne diseases on an urban environment: The effects of

heterogeneity and human circulation. *Ecological Complexity*, 30:76–90, 2017. doi:10.1016/j.ecocom.2016.12.006.

[82] G Chowell, R Fuentes, A Olea, X Aguilera, H Nesse, and J M Hyman. The Basic Reproduction Number R_0 and Effectiveness of Reactive Interventions during Dengue Epidemics: The 2002 Dengue Outbreak in Easter Island, Chile. *Mathematical biosciences and engineering*, 10(5–6):1455–1474, 2013. doi:10.3934/mbe.2013.10.1455.

[83] Ziad A Memish, Anwar Rafay, Kingsley Ukwaja, Naohiro Yonemoto, and Christopher J L Murray. The global burden of dengue: an analysis from the Global Burden of Disease Study 2013. *The Lancet Infectious Diseases*, 176(1): 100–106, 2016. doi:10.1016/S1473-3099(16)00026-8.

[84] Gobierno de México. Datos abiertos. https://www.coronavirus.gob.mx/datos/. Accessed July 19, 2020.

[85] Consejo Nacional de Población (CONAPO). Proyecciones de la población de los municipios de méxico, 2015-2030. September 2018. https://www.gob.mx/conapo/documentos/proyecciones-de-la-poblacion-de-los-municipios-de-mexico-2015-2030. Accessed August 14, 2020.

[86] Mayra R. Tocto Erazo. Shiny app script. August 2020. https://github.com/BioMatUnison/COVID-19_Proyect/tree/master/AppModel.

[87] Qianying Lin, Shi Zhao, Daozhou Gao, Yijun Lou, Shu Yang, Salihu S. Musa, Maggie H. Wang, Yongli Cai, Weiming Wang, Lin Yang, and Daihai He. A conceptual model for the coronavirus disease 2019 (COVID-19) outbreak in Wuhan, China with individual reaction and governmental action. *International Journal of Infectious Diseases*, 93:211–216, 2020. doi:10.1016/j.ijid.2020.02.058.

[88] Sijia Tian, Nan Hu, Jing Lou, Kun Chen, Xuqin Kang, Zhenjun Xiang, Hui Chen,

Dali Wang, Ning Liu, Dong Liu, Gang Chen, Yongliang Zhang, Dou Li, Jianren Li, Huixin Lian, Shengmei Niu, Luxi Zhang, and Jinjun Zhang. Characteristics of COVID-19 infection in Beijing. *Journal of Infection*, 80(4):401–406, 2020. doi:10.1016/j.jinf.2020.02.018.

[89] Stephen A. Lauer, Kyra H. Grantz, Qifang Bi, Forrest K. Jones, Qulu Zheng, Hannah R. Meredith, Andrew S. Azman, Nicholas G. Reich, and Justin Lessler. The incubation period of coronavirus disease 2019 (CoVID-19) from publicly reported confirmed cases: Estimation and application. *Annals of Internal Medicine*, 172(9):577–582, 2020. doi:10.7326/M20-0504.

[90] Shaoqing Lei, Fang Jiang, Wating Su, Chang Chen, Jingli Chen, Wei Mei, Li Ying Zhan, Yifan Jia, Liangqing Zhang, Danyong Liu, Zhong Yuan Xia, and Zhengyuan Xia. Clinical characteristics and outcomes of patients undergoing surgeries during the incubation period of COVID-19 infection. *EClinicalMedicine*, 21:100331, 2020. doi:10.1016/j.eclinm.2020.100331.

[91] Natalie Linton, Tetsuro Kobayashi, Yichi Yang, Katsuma Hayashi, Andrei Akhmetzhanov, Sung-mok Jung, Baoyin Yuan, Ryo Kinoshita, and Hiroshi Nishiura. Incubation Period and Other Epidemiological Characteristics of 2019 Novel Coronavirus Infections with Right Truncation: A Statistical Analysis of Publicly Available Case Data. *Journal of Clinical Medicine*, 9(2):538, 2020. doi:10.3390/jcm9020538.

[92] Marina Pollán, Beatriz Pérez-Gómez, Roberto Pastor-Barriuso, Jesús Oteo, Miguel A. Hernán, Mayte Pérez-Olmeda, Jose L. Sanmartín, Aurora Fernández-García, Israel Cruz, Nerea Fernández de Larrea, et al. Prevalence of SARS-CoV-2 in Spain (ENE-COVID): a nationwide, population-based seroepidemiological study. *The Lancet*, 396(10250):535–544, 2020. doi:10.1016/S0140-6736(20)31483-5.